SUPPORTING INFORMATION

Fluorination and Hydrolytic Stability of Water-Soluble Platinum Complexes with a Borane-Bridged Diphosphoramidite Ligand

Johnathan D. Culpepper,[ab] Kyounghoon Lee,[ac] William Portis,[a] Dale C. Swenson,[a] and Scott R. Daly[a]*

[a]Department of Chemistry, The University of Iowa, E331 Chemistry Building, Iowa City, Iowa 52242, United States

[b]Current address: Corning Incorporated, Corning, NY 14831, United States.

[c]Current address: Department of Chemical Education and Research Institute of Natural Sciences, Gyeongsang National University, Jinju 52828, Republic of Korea

Corresponding email: scott-daly@uiowa.edu

Table of Contents

1. Experimental

General Considerations. Reactions were carried out under an N_2 or Ar atmosphere using glovebox or standard Schlenk techniques unless stated otherwise. Glassware used for reactions performed under inert conditions was dried in an oven at 150 °C for at least 2 h and allowed to cool under vacuum before use. All solvents used were dried and deoxygenated using a Pure Process Technologies Solvent Purification System and stored over 3 Å molecular sieves under N_2. (^{MeO}TBDPhos)$PtCl_2$ (**1**) and (^{iPrO}TBDPhos)$PtCl_2$ (**3**) were prepared as described previously.[1-2] All other reagents were purchased from commercial vendors and used without further purification.

Water used for hydrolysis and solubility experiments was Millipore grade and obtained from a Milli-Q® Advantage A10® System that measured 18.2 MΩ·cm @ 25 °C with no more than 4 ppb total organic contaminants. Reported pH values were recorded on a triple point calibrated pH meter with an R^2 = 0.999. Stock solutions prepared for pH studies were lowered to the desired pH using 10 mM HCl and further adjusted with 2.5 mM NaOH as needed. NaCl used to prepare the 0.9% w/v normal saline solution was purchased from Sigma-Aldrich at 99.999% trace metal basis purity.

^{1}H, ^{13}C, ^{11}B and ^{31}P NMR data were recorded on a Bruker AVANCE (500-MHz), Bruker DRX (400-MHz) or Bruker AVANCE (300-MHz). ^{19}F NMR data were acquired on a Bruker AVANCE (500-MHz), Bruker AVANCEIII (400-MHz), or a Bruker AVANCE (300 MHz) instrument. Chemical shifts are reported in δ units in ppm referenced to residual solvent peaks (^{1}H and ^{13}C) or to 85% H_3PO_4 (^{31}P; δ 0.0 ppm), 0.05% $C_6H_5CF_3$ in C_6D_6 (^{19}F; δ -62.9), and $BF_3{\cdot}Et_2O$ (^{11}B; δ 0.0 ppm). Microanalysis data (CHN) were collected using an EAI CE-440 Elemental Analyzer at the University of Iowa's MATFab Facility. IR spectra were collected on a Thermo Scientific Nicolet iS5 using an attenuated total reflection (ATR) accessory.

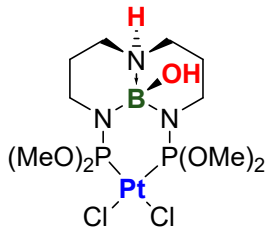

(^{MeO}TBDPhos-H_2O)$PtCl_2$ (1-H_2O). To a stirring solution of **1** (54 mg, 0.091 mmol) in CH_3CN (1.6 mL) was added H_2O (2 µL, 0.11 mmol) in air. The colorless solution was stirred for 10 minutes and evaporated to dryness under vacuum. The residue was extracted with CH_2Cl_2 (1.6 mL), filtered, and then crystallized by vapor diffusion with Et_2O to obtain colorless blocks. Yield: 22.6 mg (41%). Anal. Calcd for $C_{10}H_{26}BCl_2N_3O_5P_2Pt$: C, 19.8; H, 4.32; N, 6.92. Found: C, 19.7; H, 4.30; N, 6.81. ^{1}H NMR (400 MHz, CD_3CN, 20 °C): δ 1.64 (m, CH_2-C$\underline{H}_2$-CH_2, 4H), 2.74 (m, NCH_2, 2H), 2.87 (m, NCH_2, 2H), 3.04 (m, NCH_2, 2H), 3.43 (m, NCH_2, 2H), 3.60 (m, OCH_3, 6H), 3.76 (m, OCH_3, 6H), 4.08 (br s, CH_2-N$\underline{H}$-CH_2, 1H). ^{11}B NMR (CD_3CN, 20 °C): δ 1.2 (br s, FWHM = 70 Hz). ^{13}C{^{1}H} NMR (100.6 MHz, CD_3CN, 20 °C): δ 27.8 (s, CH_2-$\underline{C}H_2$-CH_2), 39.9 (s, NCH_2), 50.3 (s, NCH_2), 52.8 (s, OCH_3), 54.0 (s, OCH_3). ^{31}P{^{1}H} NMR (162.0 MHz, CD_3CN, 20 °C): δ 69.4 (s with doublet satellites, $^{1}J_{PtP}$ = 4938 Hz). IR (KBr, cm^{-1}): 3580 w, 3407 vw, 3135 w, 2942 w, 2887 vw, 2837 vw, 1941 vw, 1733 vw, 1701 vw, 1686 vw, 1653 vw, 1559 w, 1484 m, 1464 m, 1442 m, 1419 m, 1372 m, 1350 m, 1302 s, 1250 m, 1246 m, 1211 w, 1169 s, 1129 w, 107 vw, 1088 s, 1030 vs (PO), 975 vw, 955 vw, 926 w, 890 m, 882 vw, 882 w, 823 w, 811 m, 793 m, 760 m, 721 w, 680 vw, 678 w, 647 m, 582 w, 561 w, 560 w, 548 vw, 533 vw, 492 vw, 436 vw, 408 m, 400 vs.

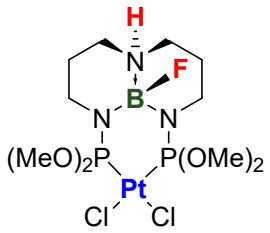

(MeOTBDPhos-HF)PtCl$_2$ (1-HF). *Method 1.* To a stirring solution of **1** (0.103 g, 0.175 mmol) in CH_3CN (3.2 mL) was added distilled water (3.16 uL, 0.175 mmol) to form **1-H$_2$O** in situ. The reaction mixture was filtered and CsF (0.027 g, 0.175 mmol) was added to the filtrate. ^{11}B, ^{31}P, and ^{19}F NMR data collected on the mixture suggested conversion to **1-HF**. ^{11}B NMR (128.4 MHz, CH_3CN, 20 °C): δ 1.2 (br s, FWHM = 130 Hz). ^{19}F NMR (376.5 MHz, CH_3CN, 20 °C): δ -166.7 (m). ^{31}P{^{1}H} NMR (161.2 MHz, CH_3CN, 20 °C): δ 69.2 (s with doublet satellites, $^1J_{Pt-P}$ = 4935 Hz). Attempts to isolate **1-HF** by vapor diffusing the CH_3CN solution with Et_2O yielded a mixture of products based on analysis of the crystallized solids.

Method 2. A solution of **1** (0.150 g, 0.26 mmol) and ($HNEt_3$)Cl (0.035 g, 0.26 mmol) in anhydrous CH_3CN (5 mL) was added to a solution of Kryptofix® 222 (0.096 g, 0.26 mmol) and KF (0.015 g, 0.26 mmol) in anhydrous CH_3CN (15 mL). The reaction mixture immediately turned yellow, and ^{19}F NMR analysis of the mixture revealed a new resonance at δ -167 ppm consistent with **1-HF**. The mixture was stirred overnight, filtered, evaporated to dryness under vacuum, and then extracted with CH_2Cl_2. Yellow crystals were obtained by vapor diffusion of Et_2O into CH_2Cl_2 solution. NMR and microanalysis data indicate that **1-HF** co-crystallizes with Kryptofix® 222·KCl. Yield: 0.103 g (66% based on formula with co-crystallized Kryptofix® 222·KCl). Anal. Calcd for $C_{10}H_{25}BCl_2FN_3O_4P_2Pt\cdot(C_{18}H_{36}ClKN_2O_6)_{1.2}$: C, 33.00; H, 5.98; N, 6.58. Found: C, 32.91; H, 6.10; N, 5.86. ^{1}H NMR (400 MHz, $CDCl_3$, 20 °C): δ 1.58 (m, CH_2-C$\underline{H}_2$-CH_2, 2H), δ 2.18 (m, CH_2-C$\underline{H}_2$-CH_2, 2H), 2.72 (m, NCH_2, 2H), 2.93 (m, NCH_2, 2H), 3.10 (m, NCH_2, 2H), 3.69 (m, OCH_3, 6H), 3.97 (m, OCH_3, 6H), δ 7.84 (br s, CH_2-N$\underline{H}$-CH_2, 1H). ^{11}B NMR (128.4 MHz, $CDCl_3$, 20 °C): δ 0.8 (br s, FWHM = 130 Hz). ^{13}C{^{1}H} NMR (100.6 MHz, $CDCl_3$, 20 °C): δ 26.4 (s, CH_2-C$\underline{H}_2$-CH_2), 39.1 (s, NCH_2), 50.0 (s, NCH_2), 52.7 (s, OCH_3), 54.0 (s, OCH_3). ^{19}F NMR (470.8 MHz, $CDCl_3$, 20 °C): δ -167.3 (m). ^{31}P{^{1}H} NMR (162.0 MHz, $CDCl_3$, 20 °C): δ 69.2 (s with doublet satellites, $^1J_{Pt-P}$ = 4918 Hz). IR (ATR, cm^{-1}): 3269 w, 3229 w, 3085 vw, 2959 vw, 2879 w, 2816 w, 2730 vw, 2159 vw, 2029 vw, 1973 vw, 1671 vw, 1616 vw, 1483 w, 1446 w, 1382 vw, 1355 m, 1295 m, 1260 m, 1159 m, 1130 s, 1098 vs, 1083 vs, 1048 s, 1017 s, 948 s, 916 m, 888 m, 814 s, 796 m, 770 s, 648 s.

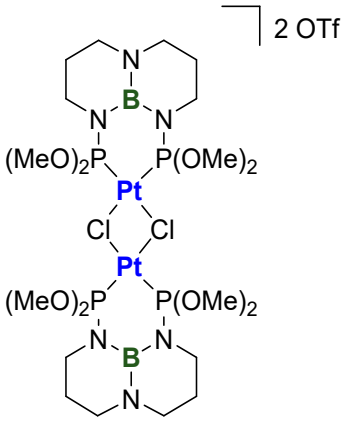

[(MeOTBDPhos)Pt(μ-Cl)]$_2$(OTf)$_2$ (2). To a stirring solution of **1** (0.20 g, 0.34 mmol) in CH_2Cl_2 (50 mL) was added AgOTf (0.087 g, 0.340 mmol). The solution was stirred overnight, filtered, and concentrated to about 2 mL. Vapor diffusion with Et_2O yielded colorless blocks. Yield: 0.199 g (83%). Anal. Calcd for $C_{22}H_{48}B_2Cl_2F_6N_6O_{14}P_4Pt_2S_2$: C, 18.80; H, 3.44; N, 5.98. Found: C, 18.93; H, 3.50; N, 6.28. ^{1}H NMR (400 MHz, $CDCl_3$, 20 °C): δ 1.90 (s, CH_2-C$\underline{H}_2$-CH_2, 8H), 3.01 (m, NCH_2, 8H), 3.29 (m, NCH_2, 8H), 3.96 (m, OCH_3, 24H). ^{11}B NMR (128.4 MHz, $CDCl_3$, 20 °C): δ 22.4 (br s, FWHM = 380 Hz). ^{13}C{^{1}H} NMR (125.8 MHz, $CDCl_3$, 20 °C): δ 25.5 (s, CH_2-C$\underline{H}_2$-CH_2), 41.0 (s, NCH_2), 48.0 (s, NCH_2), 55.4 (s, OCH_3). ^{31}P{^{1}H} NMR

(162.0 MHz, $CDCl_3$, 20 °C): δ 54.4 (s with doublet satellites, $^1J_{Pt\text{-}P}$ = 5253 Hz). ^{19}F NMR ($CDCl_3$, 20 °C): δ -78.7 (s, OTf). IR (ATR, cm^{-1}): 2948 w, 2891 vw, 2843 w, 2601 vw, 2261 vw, 2037 vw, 1526 m, 1452 w, 1389 w, 1356 w, 1332 w, 1270 s, 1256 s, 1221 s, 1186 m, 1144 m, 1091 m, 1005 vs, 935 s, 896 s, 845 m, 812 s, 761 s, 634 vs.

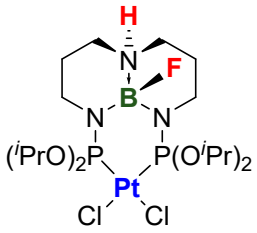

(^{iPrO}TBDPhos-HF)$PtCl_2$ (3-HF). A solution of (^{iPrO}TBDPhos)$PtCl_2$ (0.150 g, 0.214 mmol) and $(HNEt_3)Cl$ (0.0295 g, 0.214 mmol) in anhydrous CH_3CN (5 mL) was added to a solution of Kryptofix® 222 (0.081 g, 0.214 mmol) and KF (0.012 g, 0.214 mmol) in anhydrous CH_3CN (15 mL). The reaction was stirred overnight, concentrated, and then filtered. Crystals were obtained by vapor diffusion of Et_2O into the CH_3CN solution. NMR and microanalysis data indicate that **3-HF** co-crystallizes with Kryptofix® 222·KCl. Yield: 0.154 g (61% based on formula with co-crystallized Kryptofix® 222·KCl. Anal. Calcd for $C_{18}H_{41}BCl_2FN_3O_4P_2Pt{\cdot}(C_{18}H_{36}ClKN_2O_6)$: C, 36.88; H, 6.62; N, 5.97. Found: C, 36.57; H, 6.44; N, 5.94. ^1H NMR ($CDCl_3$, 20 °C): δ 1.32 (m, $OCH(CH_3)_2$, 6H), 1.41 (m, $OCH(CH_3)_2$, 12H), 1.49 (m, $OCH(CH_3)_2$, 6H), 1.60 (m, CH_2-CH_2-CH_2, 2H), 2.16 (m, CH_2-CH_2-CH_2, 2H), 2.76 (m, NCH_2, 2H), 2.92 (m, NCH_2, 2H), δ 3.11 (m, CH_2-CH_2-CH_2, 2H), 5.02 (m, $OCH(CH_3)_2$, 2H), 5.22 (m, $OCH(CH_3)_2$, 2H), 6.49 (br s, CH_2-NH-CH_2, 1H). ^{11}B NMR ($CDCl_3$, 20 °C): δ 1.1 (br s, FWHM = 120 Hz). $^{13}C\{^1H\}$ NMR ($CDCl_3$, 20 °C): δ 23.0 (s, $OCH(CH_3)_2$), 24.1 (s, $OCH(CH_3)_2$), 24.4 (s, $OCH(CH_3)_2$), 24.7 (s, $OCH(CH_3)_2$), 26.1 (s, CH_2-CH_2-CH_2), 40.2 (s, NCH_2), 50.3 (s, NCH_2), 70.7 (s, $OCH(CH_3)_2$), 71.4 (s, $OCH(CH_3)_2$). ^{19}F NMR ($CDCl_3$, 20 °C): δ -167.0 (m). $^{31}P\{^1H\}$ NMR ($CDCl_3$, 20 °C): (s) δ 59.5 (s with doublet satellites, $^1J_{PtP}$ = 4903 Hz). IR (ATR, cm^{-1}): 2970 w, 2924 w, 2880 w, 2813 w, 2735 vw, 2068 vw, 1471 w, 1444 w, 1383 w, 1355 w, 1301 w, 1250 w, 1224 vw, 1199 vw, 1093 s, 1054 s, 1011 m, 965 s, 945 s, 882 s, 828 m, 806 m, 764 s, 647 s.

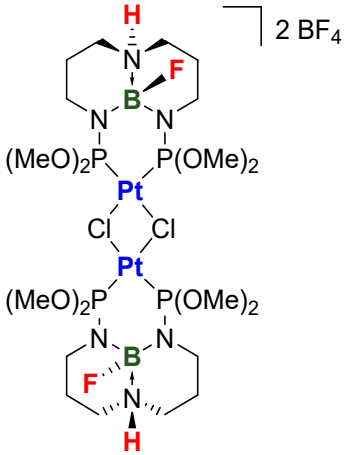

[(^{MeO}TBDPhos-HF)Pt(μ-Cl)]$_2$(BF_4)$_2$ (4-HF). To a stirring solution of **1** (0.20 g, 0.340 mmol) in CH_2Cl_2 (10 mL) was added $HBF_4{\cdot}Et_2O$ (0.11 g, 0.68 mmol). The reaction was stirred overnight, concentrated to 5 mL, and crystallized by vapor diffusion with Et_2O to yield colorless blocks. Yield: 0.17 g (76%). ^1H NMR ($CDCl_3$, 20 °C): δ 1.73 (m, 4H), 2.09 (m, 4H), 2.87 (m, 4H), 2.96 – 3.26 (m, 8H), 3.51 (m, 4H), 3.76 (m, OCH_3, 12H), 3.91 (m, OCH_3, 12H), 5.39 (s, NH, 2H). ^{11}B NMR ($CDCl_3$, 20 °C): δ -1.3 (s, BF_4^-), 0.3 (br s, FWHM = 130 Hz, N_3BF). $^{13}C\{^1H\}$ NMR ($CDCl_3$, 20 °C): δ 25.9 (s), 39.7 (s), 50.2 (s), 53.8 (s), 54.7 (s). ^{19}F NMR ($CDCl_3$, 20 °C): δ -151.8 (s, BF_4^-), -167.7 (br s, FWHM = 170 Hz, N_3BF). $^{31}P\{^1H\}$ NMR ($CDCl_3$, 20 °C): δ 51.8 (s,

$^1J_{PtP}$ = 5250 Hz). IR (ATR, cm^{-1}): 3150 w, 2943 w, 2888 w, 2823 w, 2733 vw, 1460 w, 1357 w, 1247 s, 1222 m, 1132 s, 1098 s, 1049 s, 1012 vs, 946 s, 888 s, 815 s, 770 s, 636 s.

2. Crystallographic data and molecular structures

Single crystals of **1-H_2O**, **2**, and **3-HF·(Kryptofix® 222·KCl)** were obtained from CH_2Cl_2/Et_2O and mounted on a MiTeGen micromount using ParatoneN oil in air. The data collection, structural solution, and refinement were carried out as reported previously.[3] Briefly, the structures were solved with intrinsic phasing (SHELXT)[4] and non-hydrogen atoms were confirmed with least-square method (SHELXL).[5] The final refinement included anisotropic temperature factor on all non-hydrogen atoms. Structure solution and refinement were performed with Olex[2] and publication figures were generated with Mercury.[6-7] All three structures had significant disorder, and details of how the disorder was modeled for each complex are described in detail below.

1-H_2O was modeled in the $P2_1$ space group as racemic twins. Each structure contained four crystallographically unique $P(OMe)_2$ groups that were disordered and modeled over two positions. The relative occupancies of the disordered components were constrained to equal 1.0. The P-N, P-O, O-C, B-O, B-N(H), and B-N(P) distances were restrained to be the same. The anisotropic parameters of the P, O, and C atoms in the $P(OMe)_2$ groups were subjected to isotropic constraints.

2. Two of the three triflate anions are situated near a 2-fold axes and were disordered by symmetry and assigned an occupancy of 0.5. The S111 - F118 triflate was modelled with two orientations (the second is S11' - F18') of 0.25 occupancy to better fit the large anisotropy in the displacement parameters. The two orientations' conformations were restrained to be the same and the anisotropic displacement parameters were restrained with the rigid bond restraint and similarity restraint. Due to close proximity (<0.15 Å), the displacement parameters of S111 were constrained to be the same as those of S11'. The anisotropic displacement parameters of the S121 - F128 triflate anion were also restrained with the rigid bond and similarity restraints. The S-O, S-C, C-F bonds and the O···O, F···F, S···F and C···O non-bonding distances were restrained to be the same for all the triflate anions.

The B1-containing ligand showed disorder in the C(1,2,3,5,6) positions. The N1-C1, C1-C2, C2-C3, C3-N3 and N1-C1', C1'-C2', C2'-C3', C3'-N3 bonds, respectively, were restrained to be the same as were the N2-C6, C6-C5, C5-C4 and N2-C6', C6'-C5', C5'-C4 bonds. The relative occupancies of the disordered components were constrained to equal 1.0. The relative occupancies refined to 0.745(19):0.255(19) for the major and minor (primed labels) disorder conformations. The minor disorder atoms were assigned isotropic displacement parameters equal to the U(iso, equiv) of the corresponding atom of the major conformation.

Peaks in a difference density map calculated near the end of refining were situated near a 2-fold axis and modelled as an acetonitrile solvent molecule of inclusion with partial occupancy. The N-C bond was restrained to 1.10 Å, C-C bond to 1.45 Å, and the C···C non-bonding distance to 2.65 Å. The same isotropic displacement parameter was used for all three atoms and the occupancy was fixed at 0.3 as refining both resulted in a high correlation parameter and a non-positive displacement parameter. The 0.3 occupancy give a reasonable displacement parameter.

We note that there is evidence of an unidentifiable twin in the diffraction pattern that may be unfavorably affecting the secondary weighting parameter.

3-HF·[(Kryptofix® 222)KCl]. The cryptand was disordered over two positions with the relative occupancies constrained to sum to 1.0. The two parts were restrained to have the same conformation (SAME restraint) and the anisotropic displacement parameters of the two parts were subjected to rigid bond and similarity restraints (RIGU and SIMU). A rigid bond restraint was applied to the anisotropic displacement parameters of the co-crystallized Et_2O.

Table S1. Crystallographic data for (^{MeO}TBDPhos-H_2O)$PtCl_2$ (**1-H_2O**), [(^{MeO}TBDPhos)Pt(μ-Cl)]$_2$(OTf)$_2$ (**2**), and **3-HF·(Kryptofix® 222·KCl)**.

	1-H_2O	**2**	**3-HF·(Kryptofix® 222·KCl)**
Formula	$C_{10}H_{26}BCl_2N_3O_5P_2Pt$	$C_{22}H_{48}B_2Cl_2F_6N_6O_{14}P_4Pt_2S_2$	$C_{58}H_{128}B_2Cl_5F_2KN_8O_{15}P_4Pt_2$
FW (g mol^{-1})	607.08	1405.36	1967.71
crystal system	monoclinic	orthorhombic	monoclinic
space group	$P2_1$	Aea2	C2/c
a (Å)	8.0870(11)	25.9286(8)	84.172(8)
b (Å)	14.6292(12)	18.9042(4)	10.5703(11)
c (Å)	16.036(3)	18.5116(4)	19.8514(19)
α (deg)	90	90	90
β (deg)	94.505(7)	90	103.243(5)
γ (deg)	90	90	90
volume (Å^3)	1891.3(4)	9073.6(4)	17193(3)
Z	4	8	8
ρ_{calc} (g cm^{-3})	2.132	2.058	1.520
μ (mm^{-1})	7.896	6.598	3.592
F(000)	1176	5440	8000
θ range (deg)	2.53/24.99	2.16/25.00	1.943/26.407
R(int)	0.0364	0.0711	0.0590
data/restraints/parameters	6500/1257/618	7975/807/703	17567/1484/1129
GOF	1.290	1.130	1.119
R_1 [$I > 2\sigma(I)$][a]	0.0450	0.0326	0.0478
wR_2 (all data)[b]	0.0902	0.0688	0.1110
Ext. Coeff	-	-	-
Largest Peak/Hole (e·Å^{-3})	3.09/-1.90	1.33/-1.60	1.404/-1.725
Temp (K)	100(2)	150(2)	150(2)

[a] $R_1 = \sum |F_o| - |F_c| \, | \, / \, | \sum |F_o|$ for reflections with $F_o^2 > 2\,\sigma(F_o^2)$.

[b] $wR_2 = [\sum w(F_o^2 - F_c^2)^2 \, / \, \sum (F_o^2)^2]^{1/2}$ for all reflections.

3. NMR spectra

3.1. NMR spectra of isolated complexes

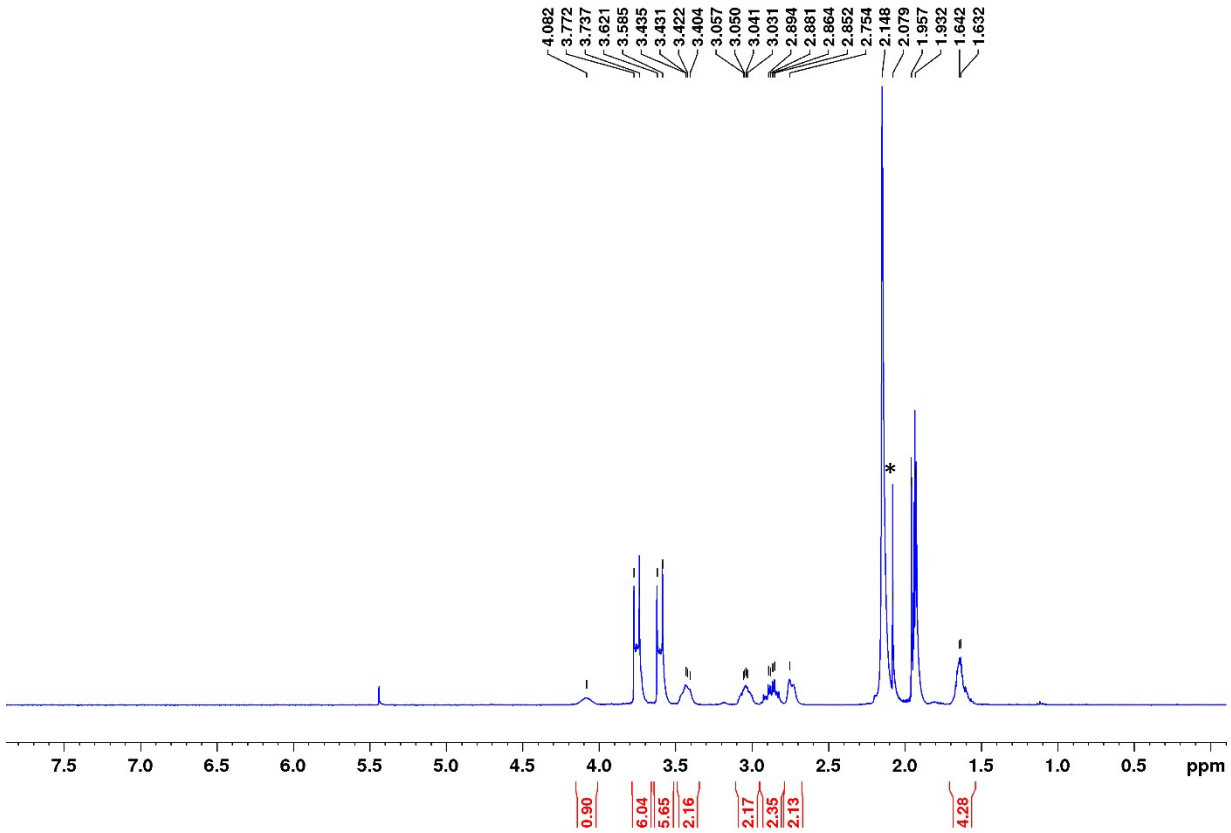

Figure S1. ^{1}H NMR spectrum of (^{MeO}TBDPhos-H_2O)$PtCl_2$ (**1-H_2O**) in CD_3CN. The peak marked with an asterisk is assigned to an acetone impurity.

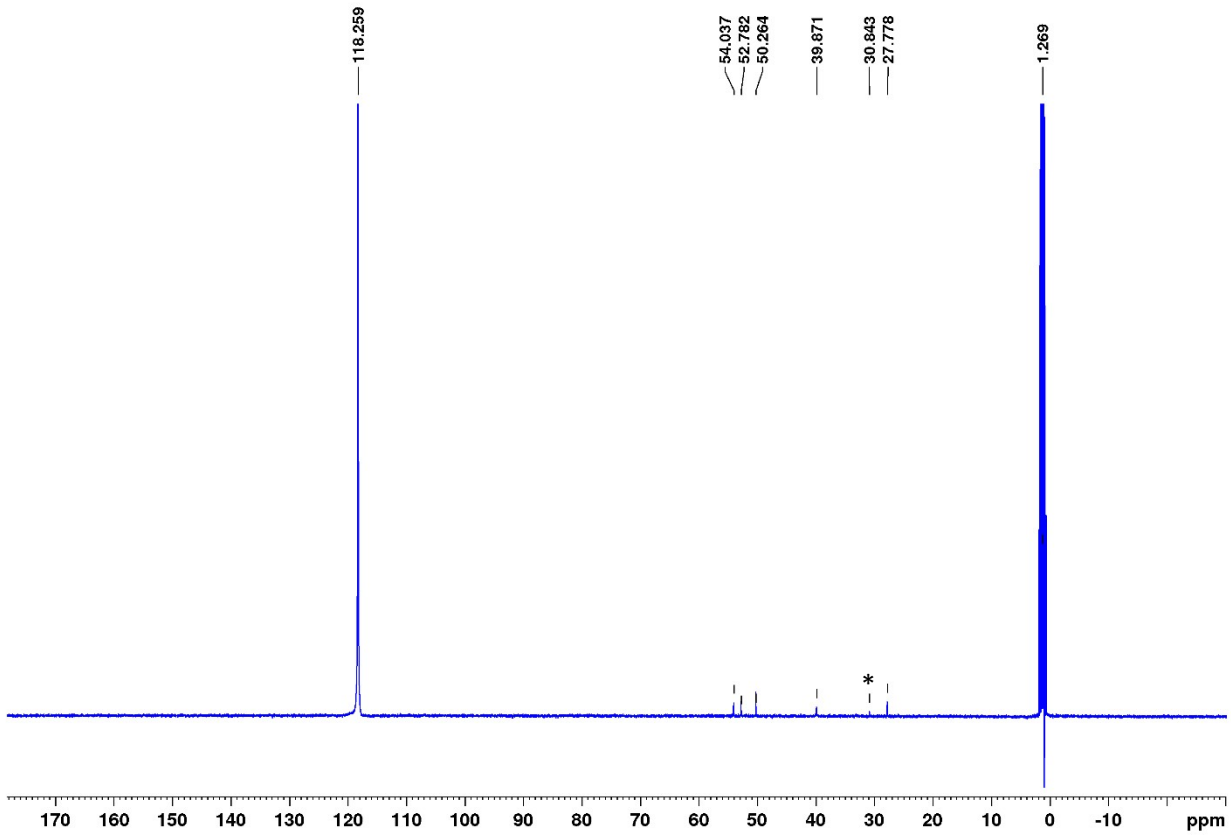

Figure S2. ^{13}C NMR spectrum of (^{MeO}TBDPhos-H_2O)$PtCl_2$ (**1-H_2O**) in CD_3CN. The peak marked with an asterisk is assigned to an acetone impurity.

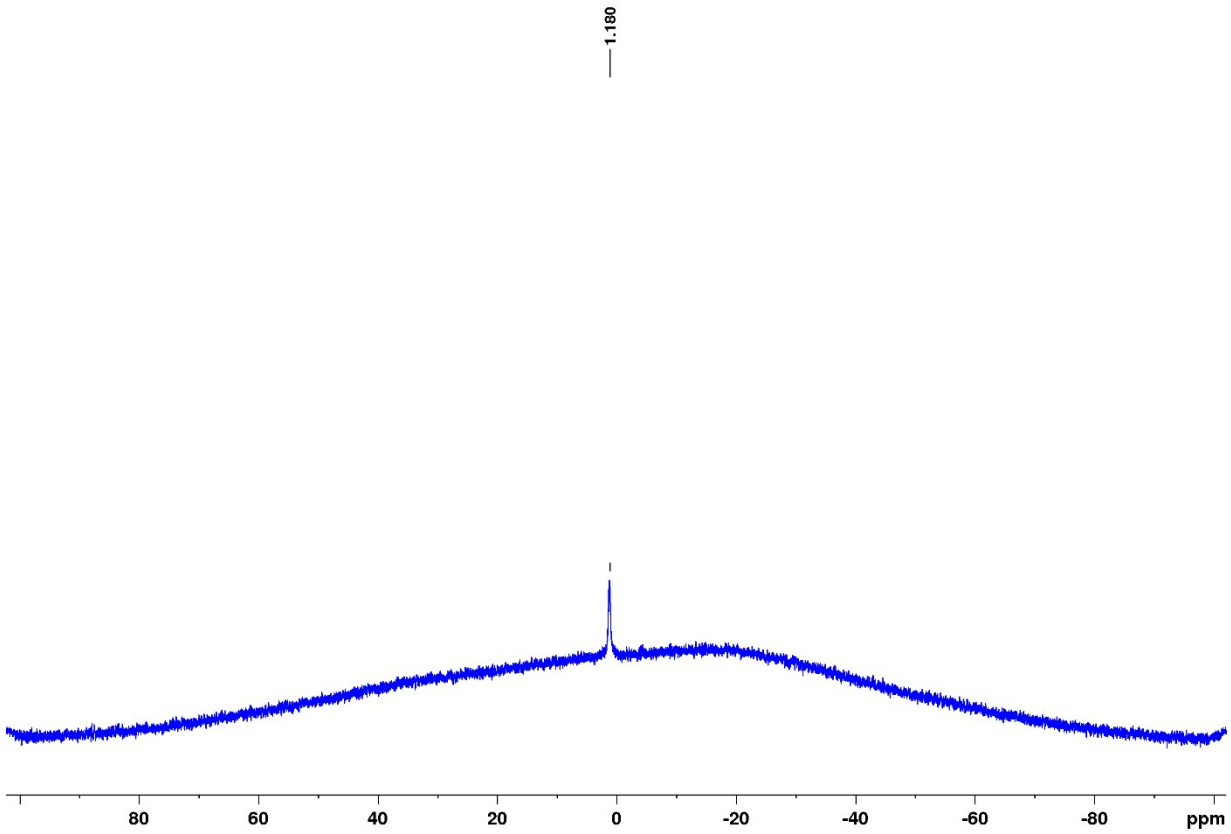

Figure S3. ^{11}B NMR spectrum of (^{MeO}TBDPhos-H_2O)$PtCl_2$ (**1-H_2O**) in CD_3CN in CD_3CN.

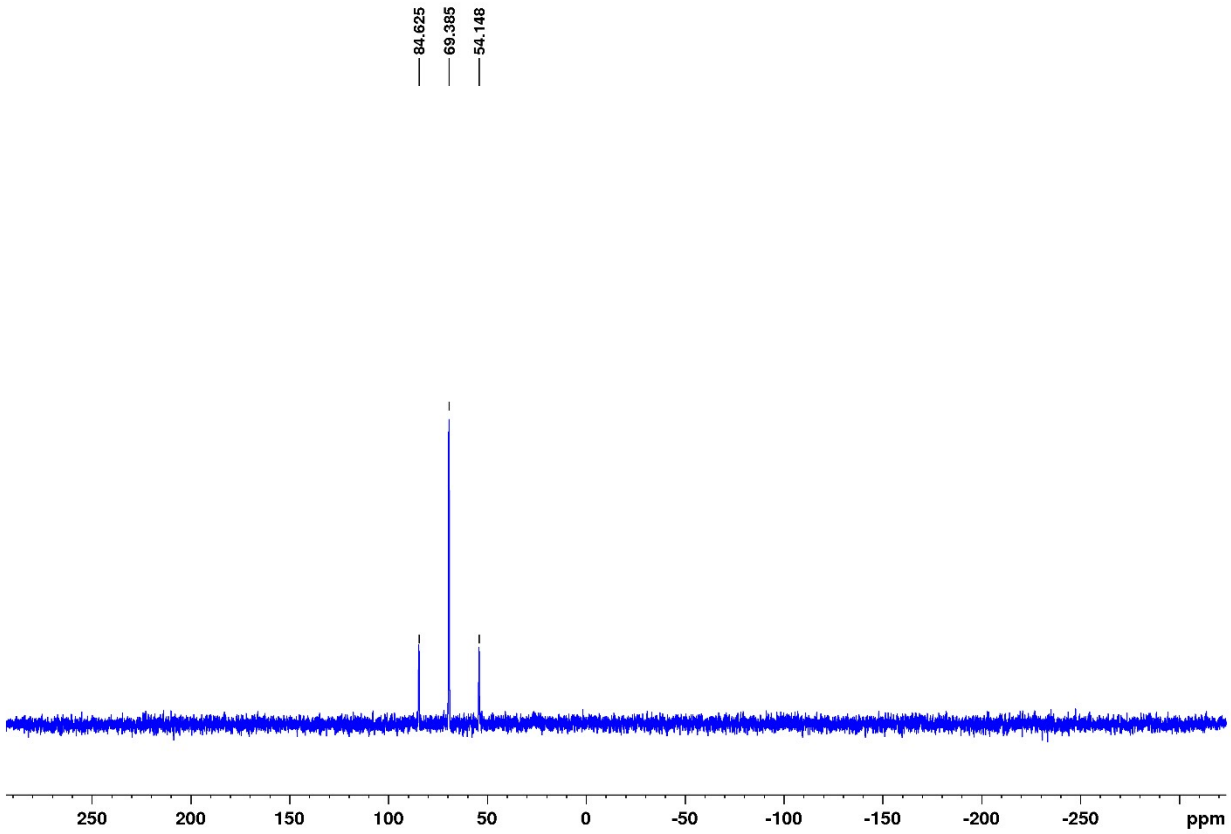

Figure S4. ^{31}P NMR spectrum of (^{MeO}TBDPhos-H_2O)$PtCl_2$ (**1-H_2O**).

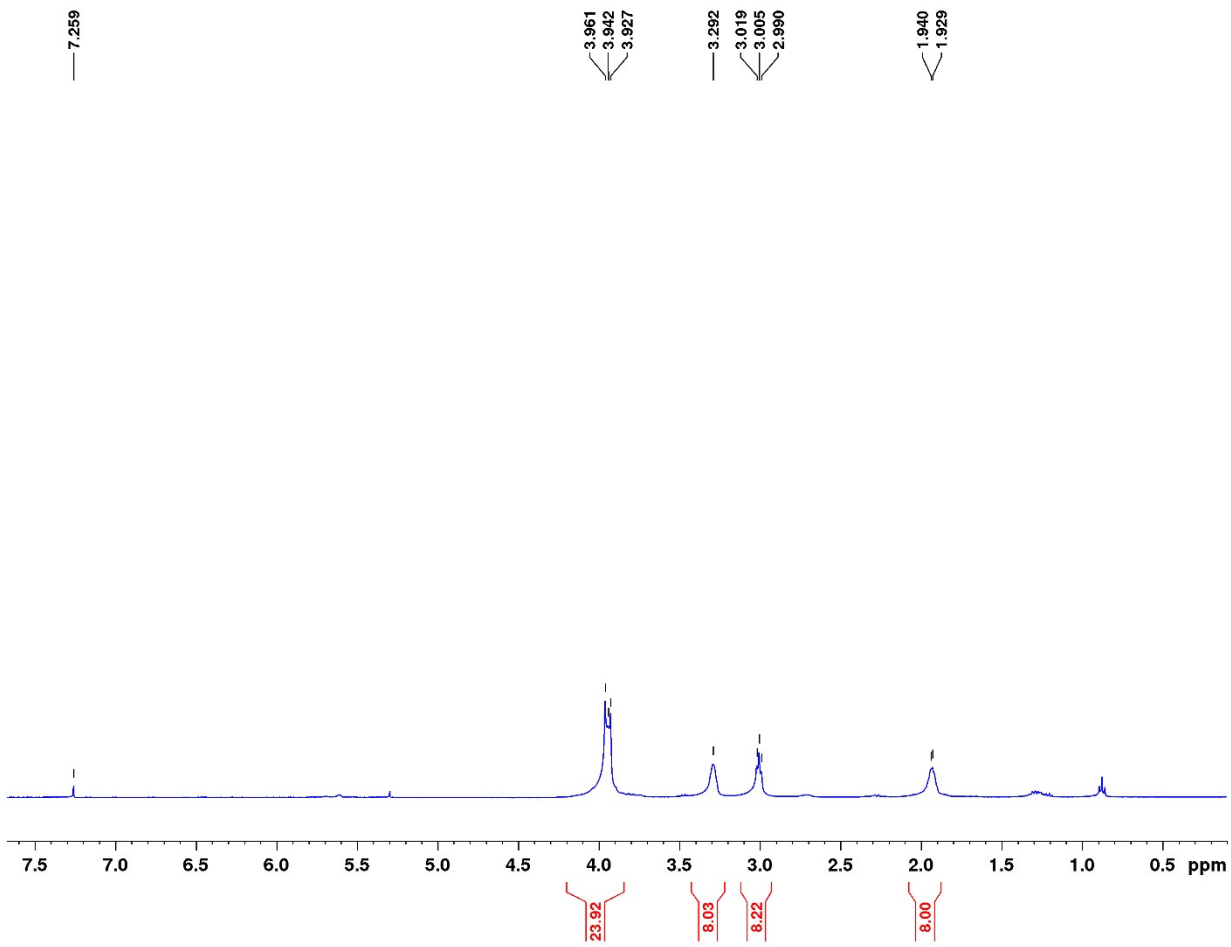

Figure S5. ^{1}H NMR spectrum of $[(^{MeO}TBDPhos)Pt(\mu\text{-}Cl)]_2(OTf)_2$ (**2**) in $CDCl_3$.

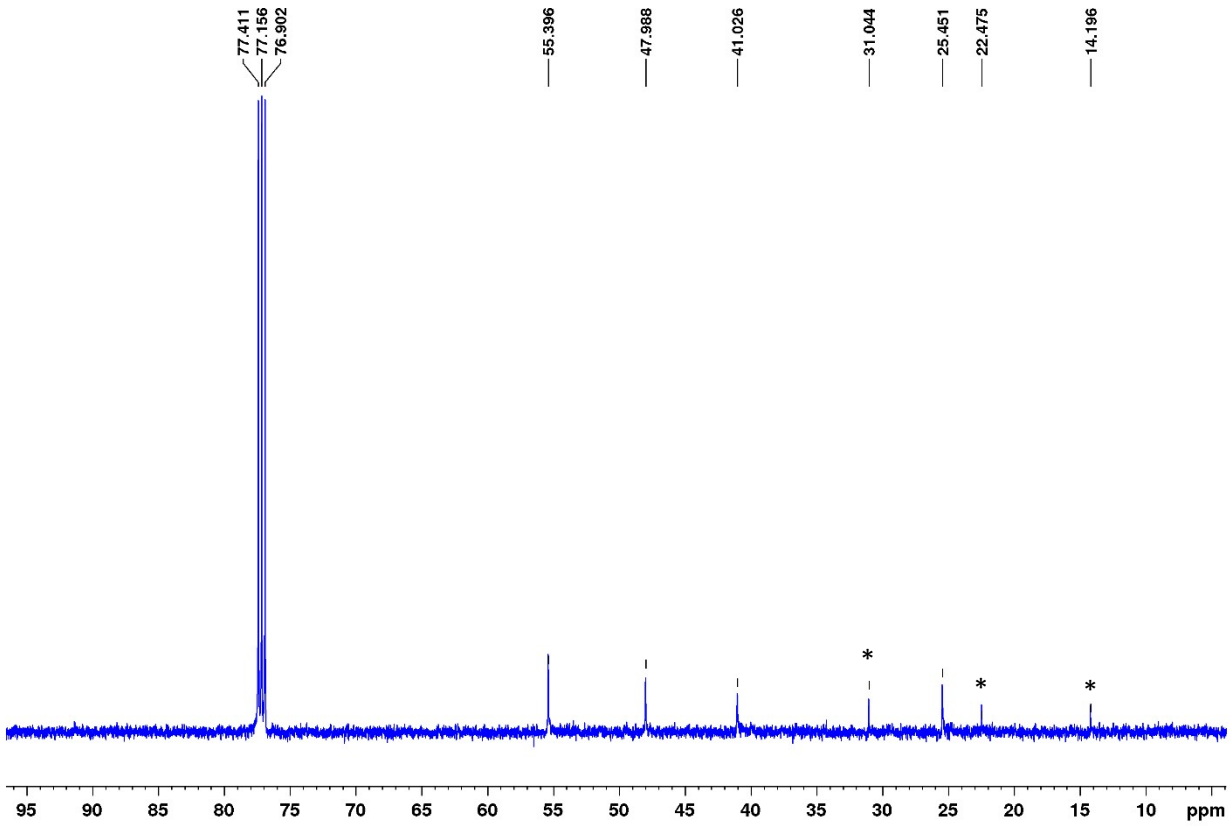

Figure S6. ^{13}C NMR spectrum of $[(^{MeO}TBDPhos)Pt(\mu\text{-}Cl)]_2(OTf)_2$ (**2**) in $CDCl_3$. The peaks marked with an asterisk are assigned to residual acetone and hexane impurities. The sample was too dilute to resolve the CF_3 resonances from the triflate anion (the ^{19}F spectrum shown below confirmed its presence).

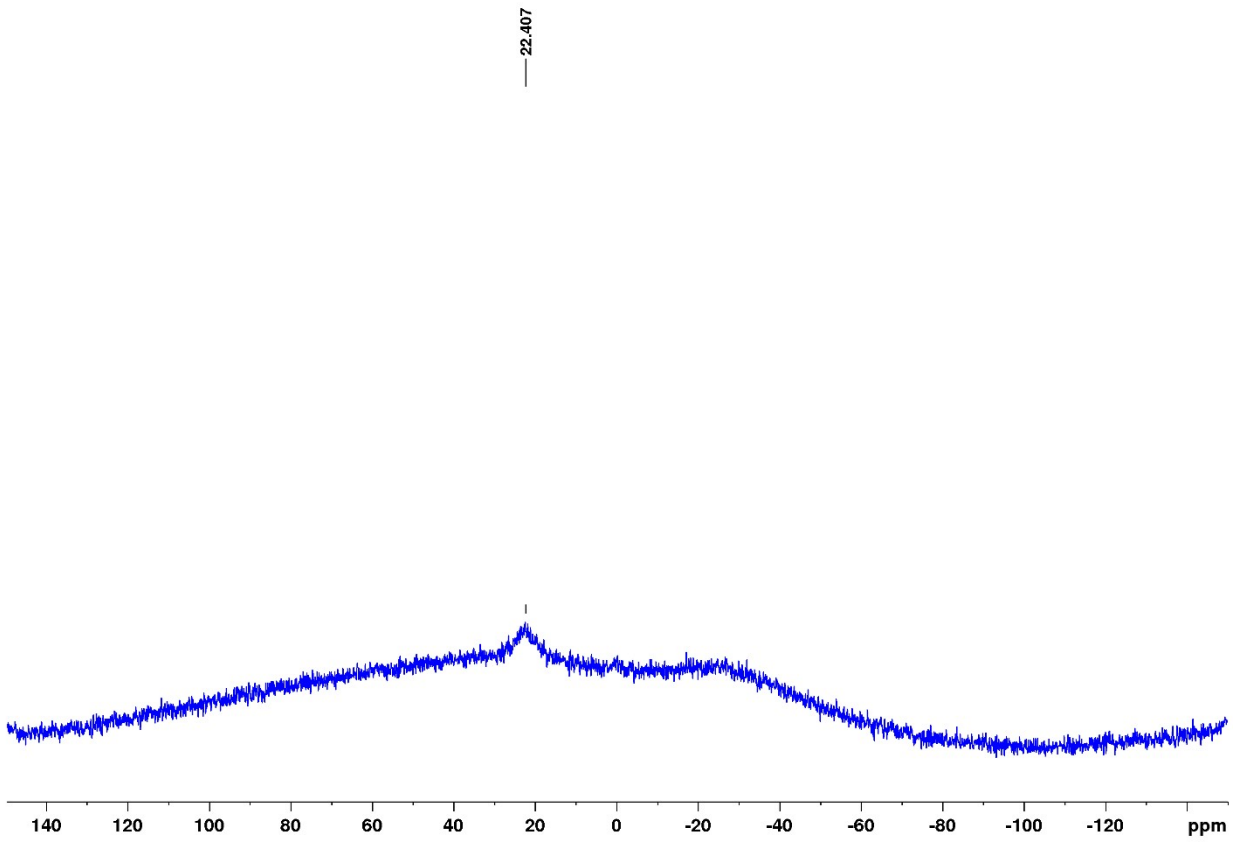

Figure S7. ^{11}B NMR spectrum of $[(^{MeO}TBDPhos)Pt(\mu\text{-}Cl)]_2(OTf)_2$ (**2**) in $CDCl_3$.

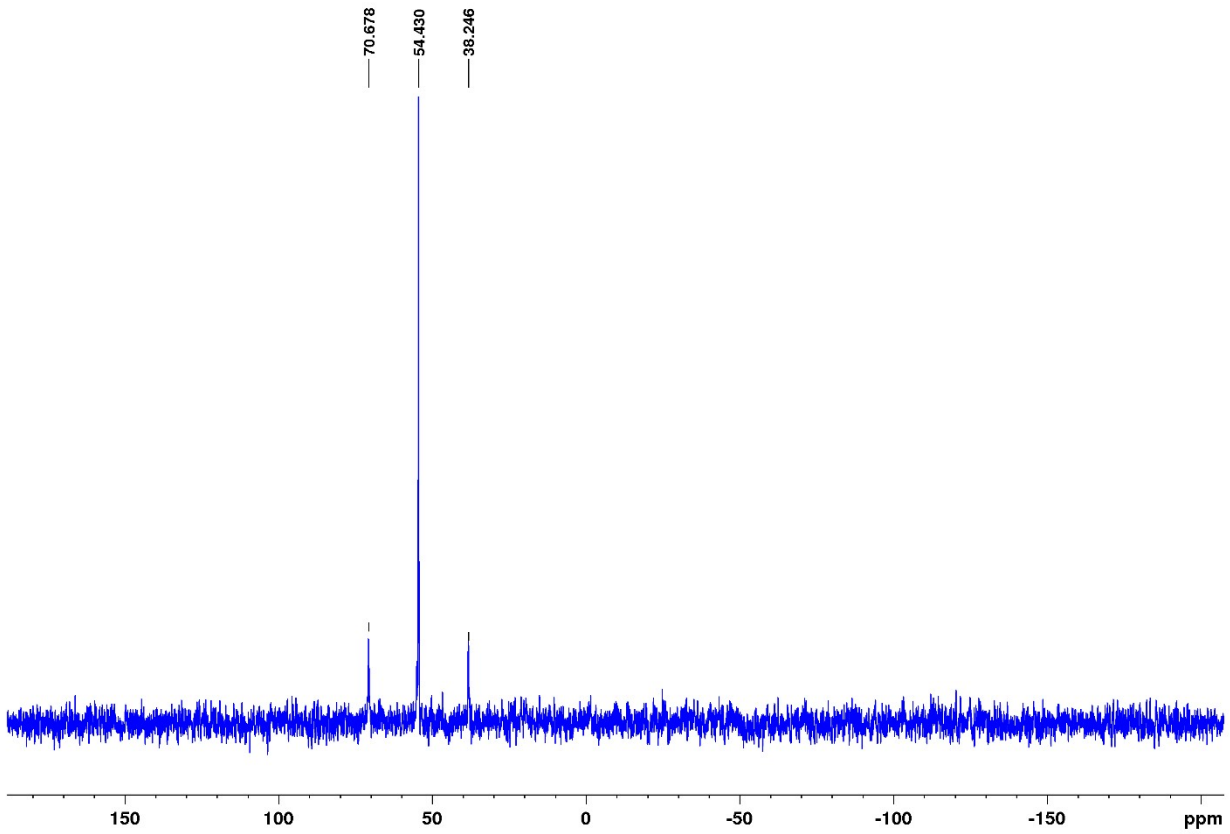

Figure S8. ^{31}P NMR spectrum of [(^{MeO}TBDPhos)Pt(μ-Cl)]$_2$(OTf)$_2$ (**2**) in $CDCl_3$.

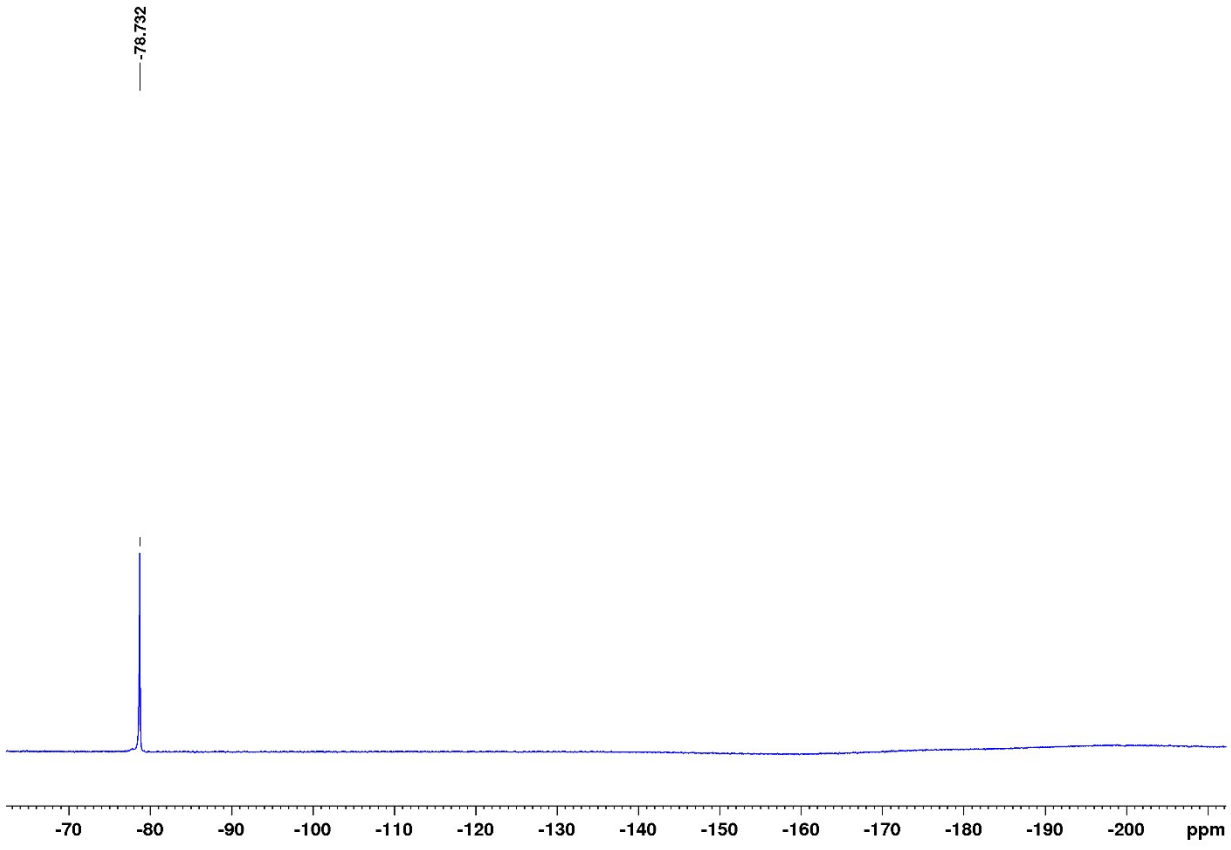

Figure S9. ^{19}F NMR spectrum of [(^{MeO}TBDPhos)Pt(μ-Cl)]$_2$(OTf)$_2$ (**2**) in $CDCl_3$.

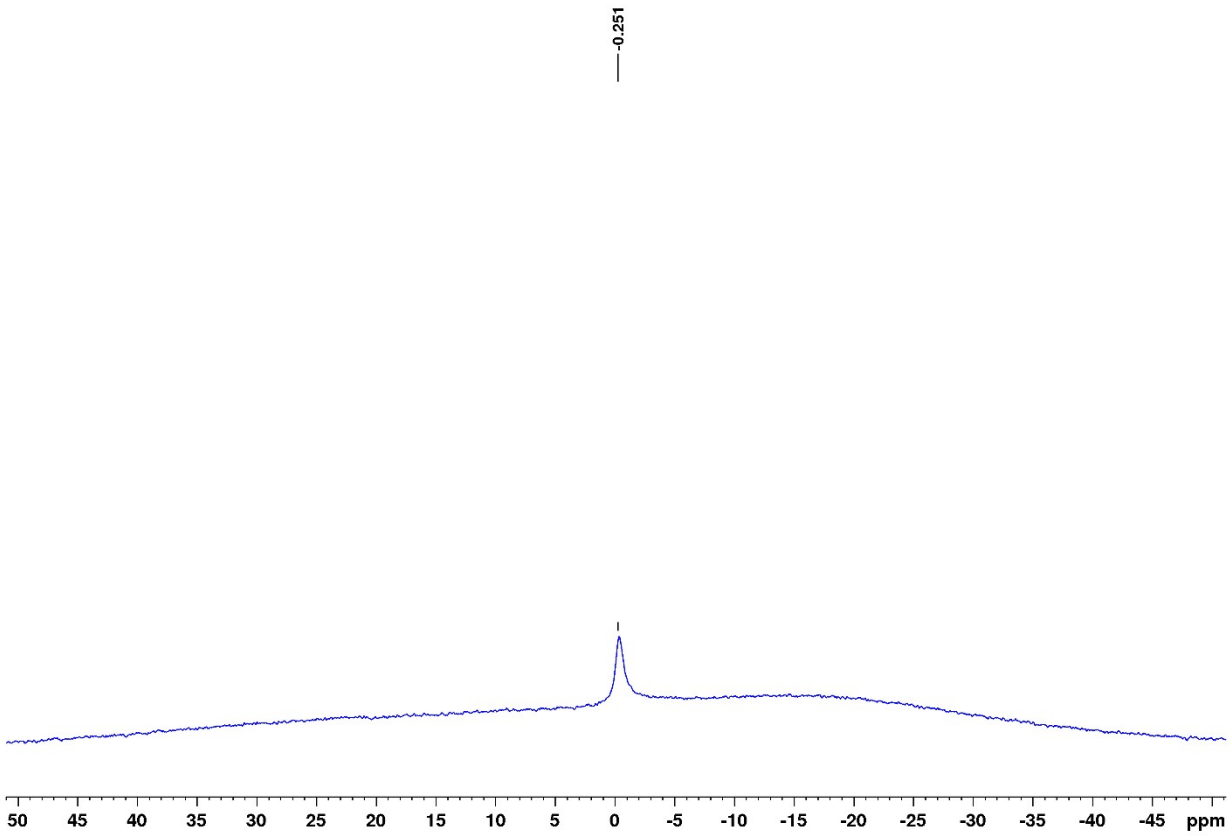

Figure S10. ^{11}B NMR spectrum of [(^{MeO}TBDPhos-H_2O)Pt(μ-Cl)]$_2$(OTf)$_2$ (**2-H_2O**) in $CDCl_3$.

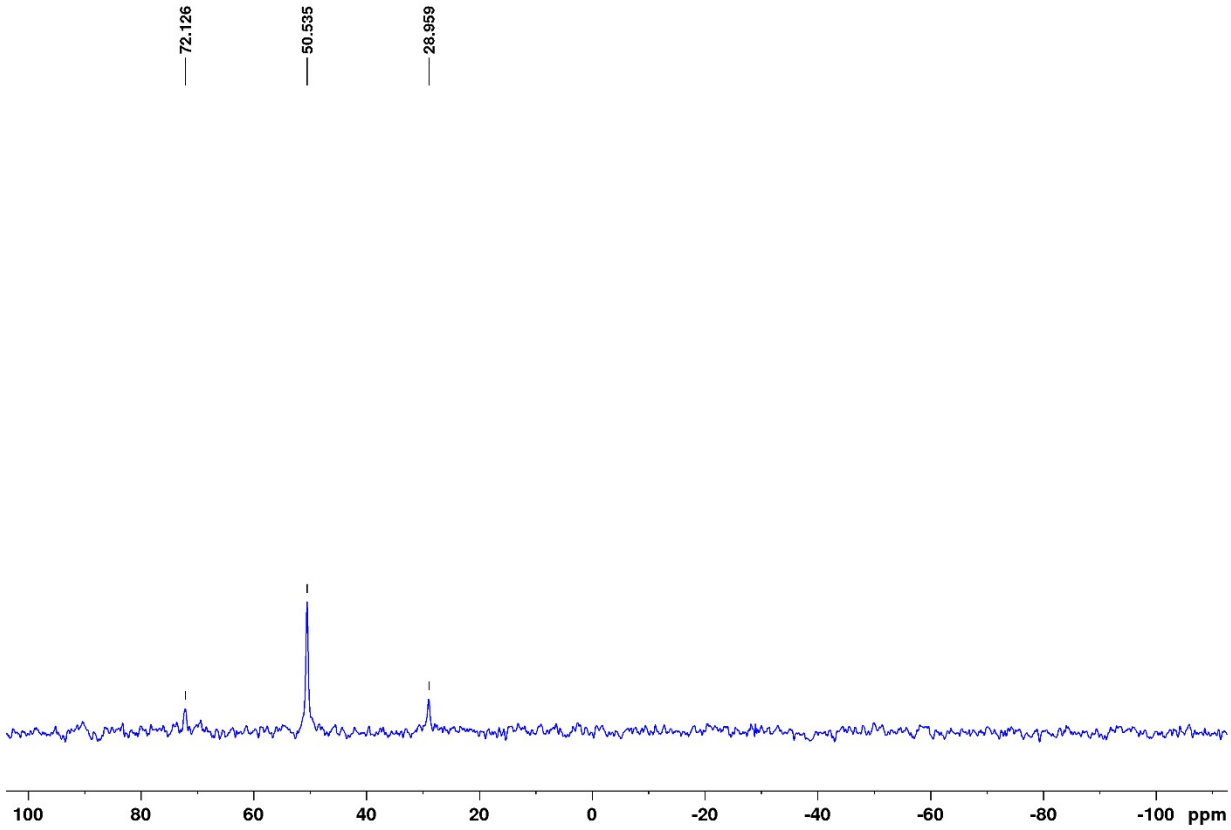

Figure S11. ^{31}P NMR spectrum of [(^{MeO}TBDPhos-H_2O)Pt(μ-Cl)]$_2$(OTf)$_2$ (**2-H_2O**) in $CDCl_3$

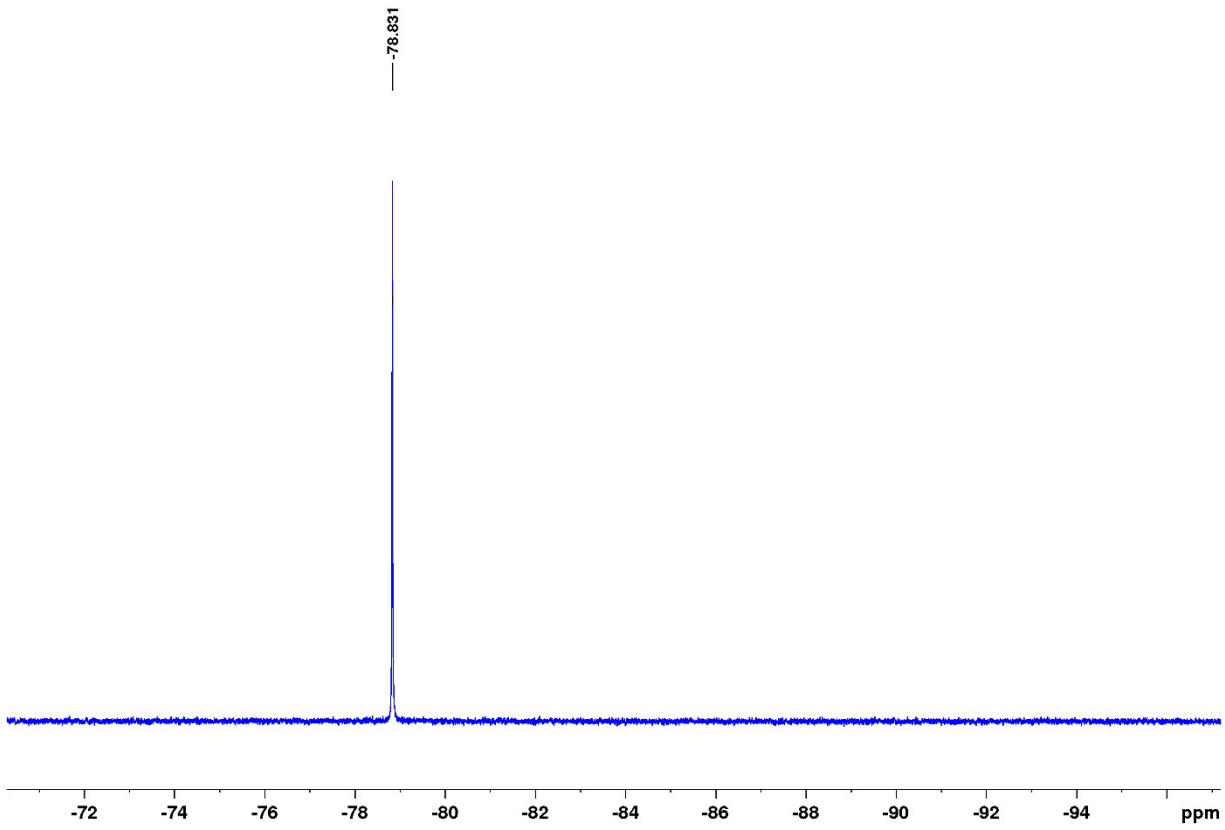

Figure S12. ^{19}F NMR spectrum of [(^{MeO}TBDPhos-H_2O)Pt(μ-Cl)]$_2$(OTf)$_2$ (**2-H_2O**) in $CDCl_3$.

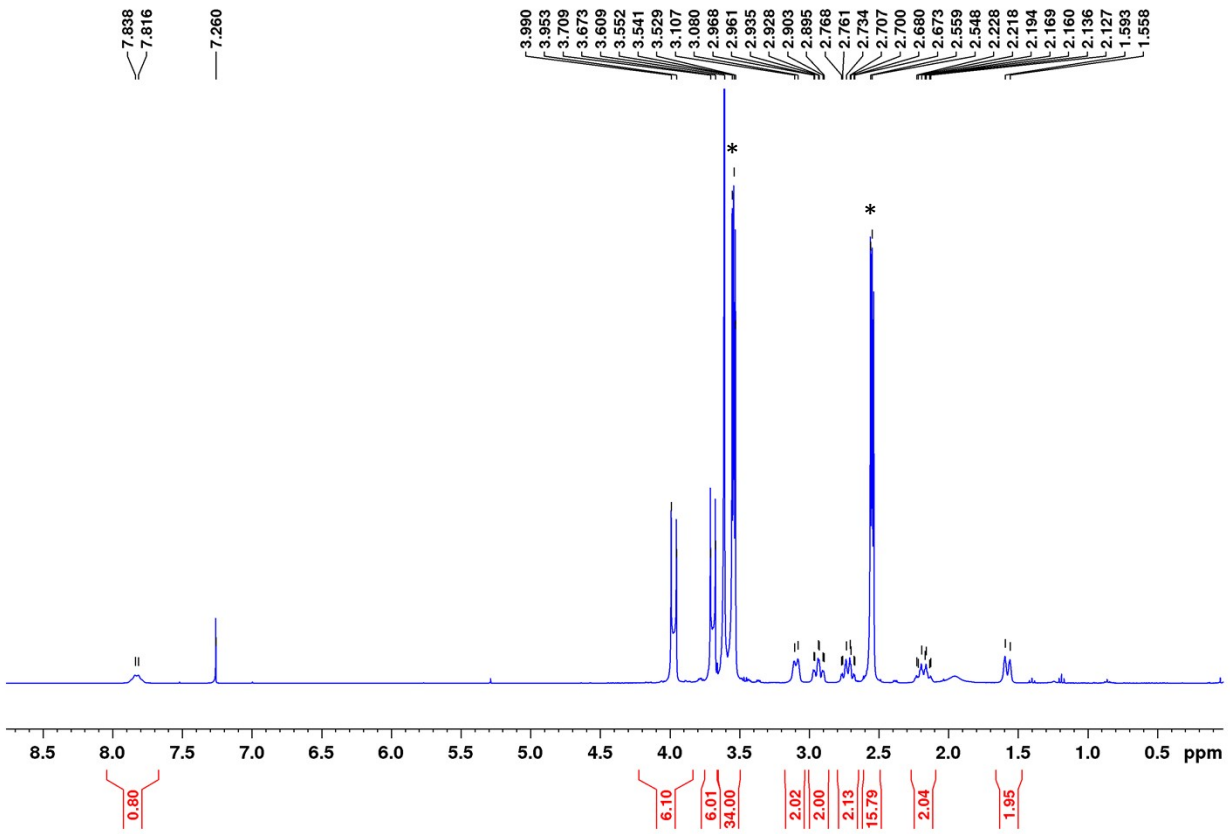

Figure S13. ^{1}H NMR spectrum of (^{MeO}TBDPhos-HF)$PtCl_2$ (**1-HF**) in $CDCl_3$. The reaction byproduct Kryptofix 222®·KCl co-crystalizes with the sample, and resonances associated with Kryptofix 222® are assigned with an asterisk.

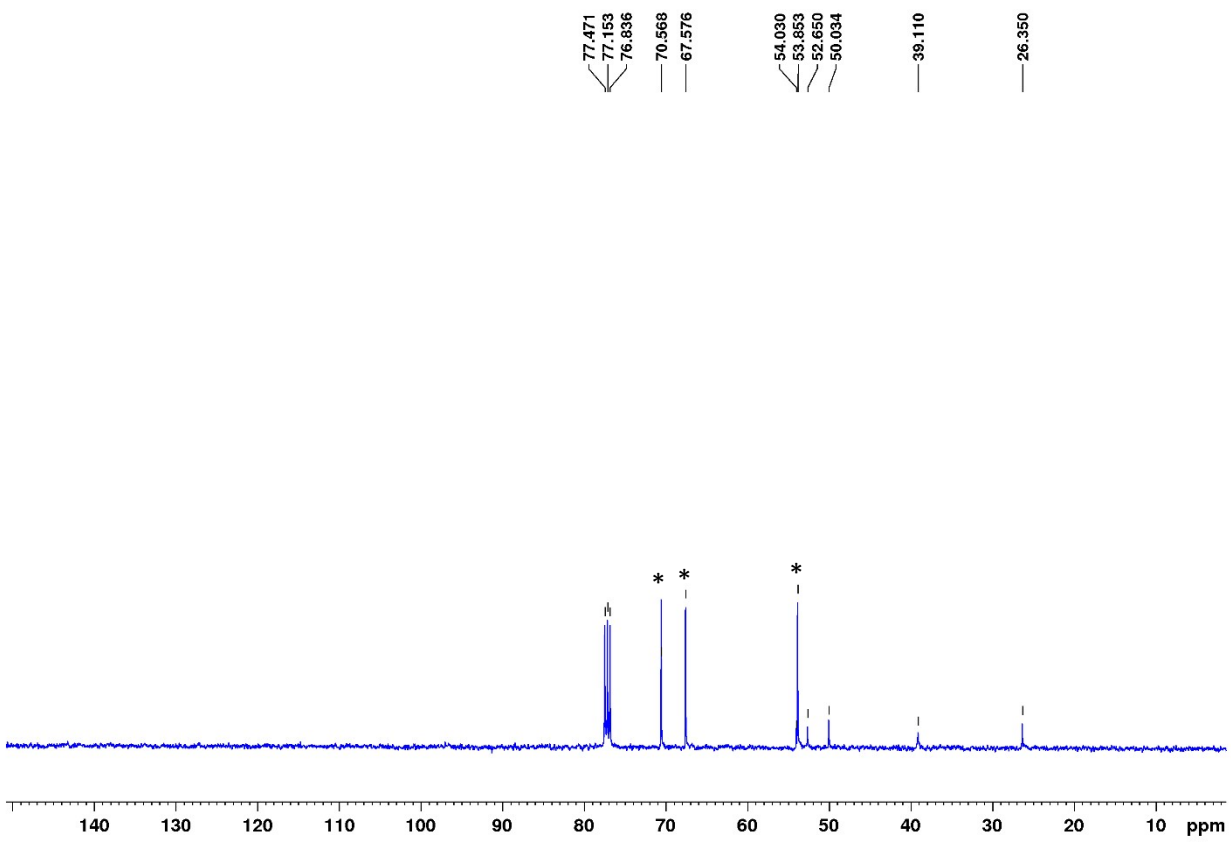

Figure S14. ^{13}C NMR spectrum of (^{Meo}TBDPhos-HF)$PtCl_2$ (**1-HF**) in $CDCl_3$. The reaction byproduct Kryptofix 222®·KCl co-crystalizes with the sample, and resonances associated with Kryptofix 222® are assigned with an asterisk.

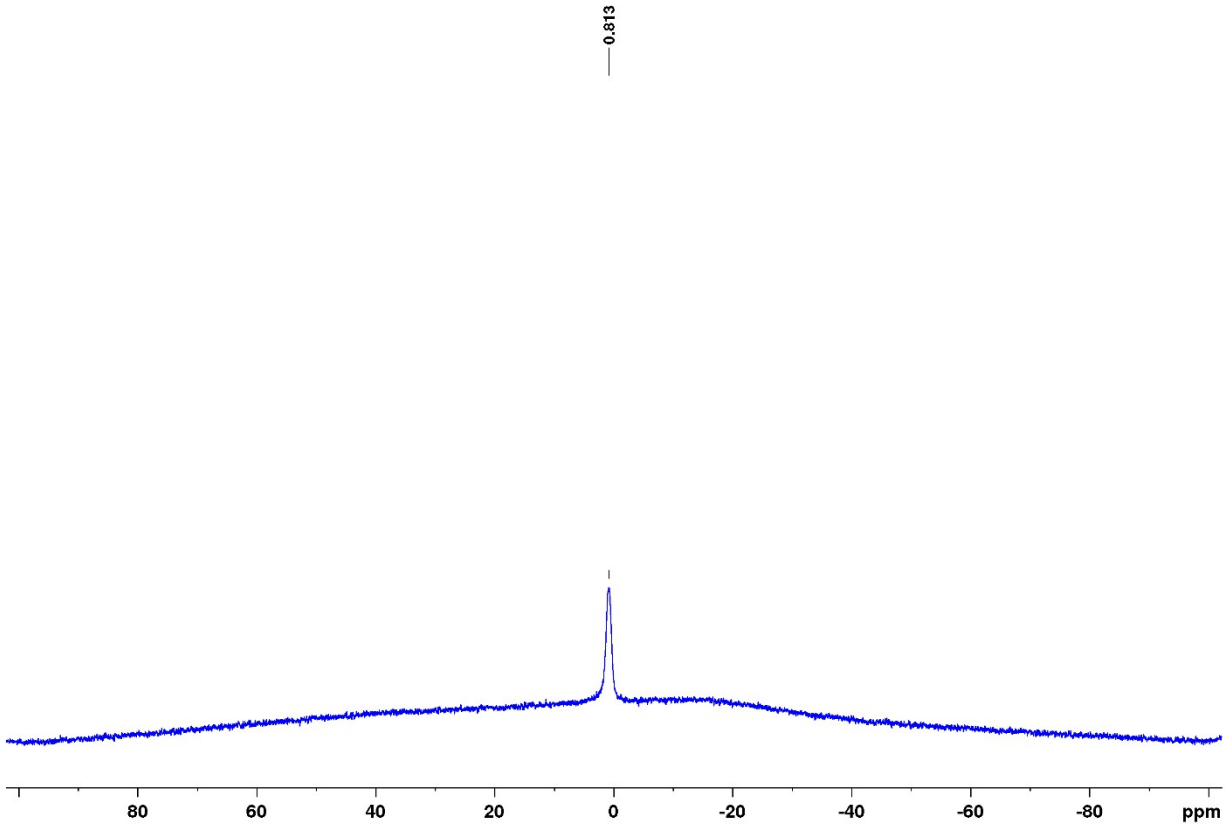

Figure S15. ^{11}B NMR spectrum of (^{MeO}TBDPhos-HF)$PtCl_2$ (**1-HF**) in $CDCl_3$.

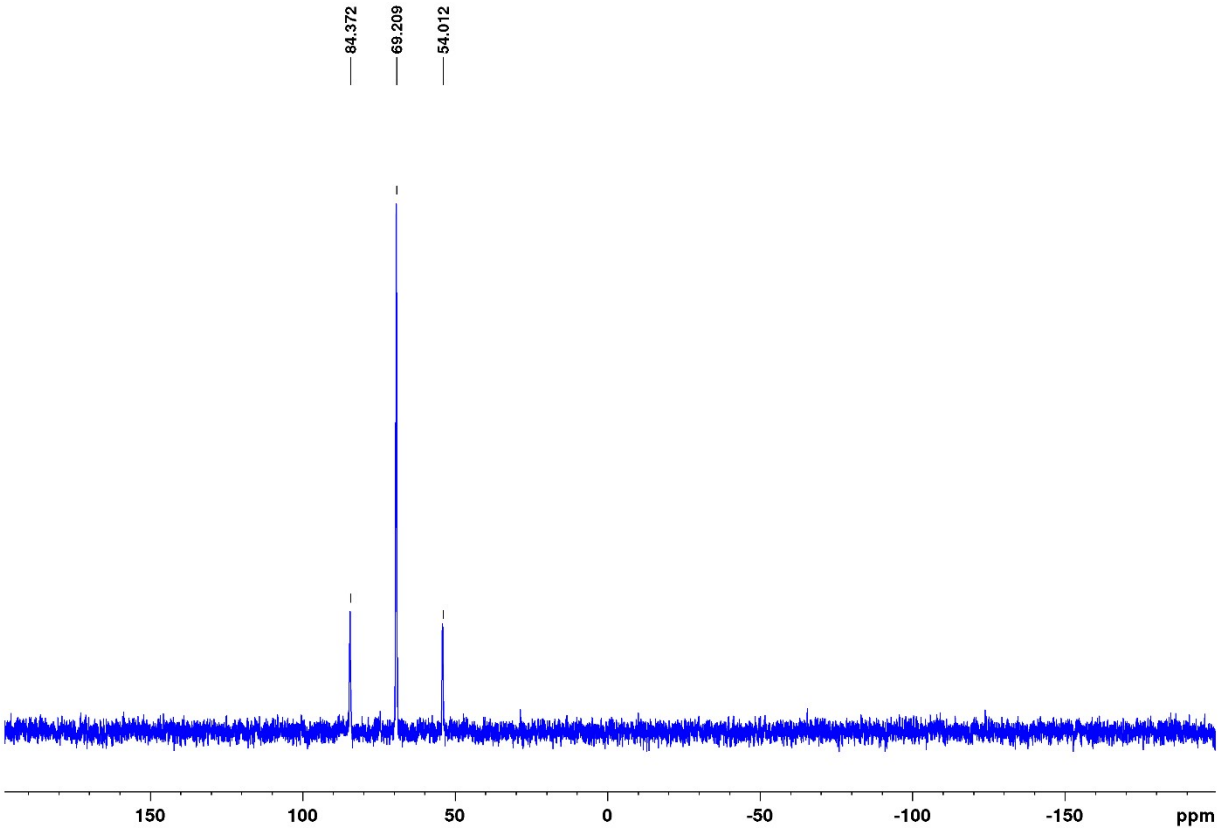

Figure S16. ^{31}P NMR spectrum of (^{MeO}TBDPhos-HF)$PtCl_2$ (**1-HF**) in $CDCl_3$.

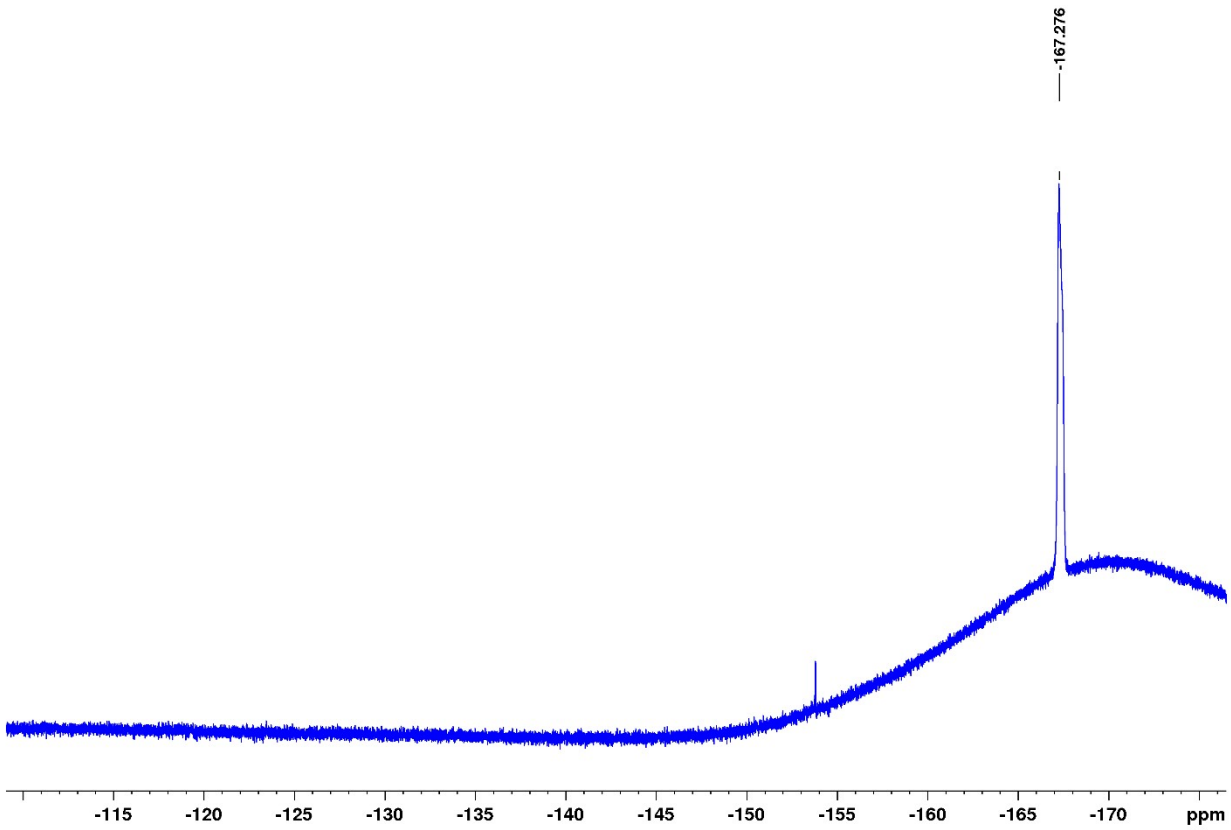

Figure S17. ^{19}F NMR spectrum of (^{MeO}TBDPhos-HF)$PtCl_2$ (**1-HF**) in $CDCl_3$. The resonance at δ -153.8 ppm is assigned to a minor B-F containing impurity.

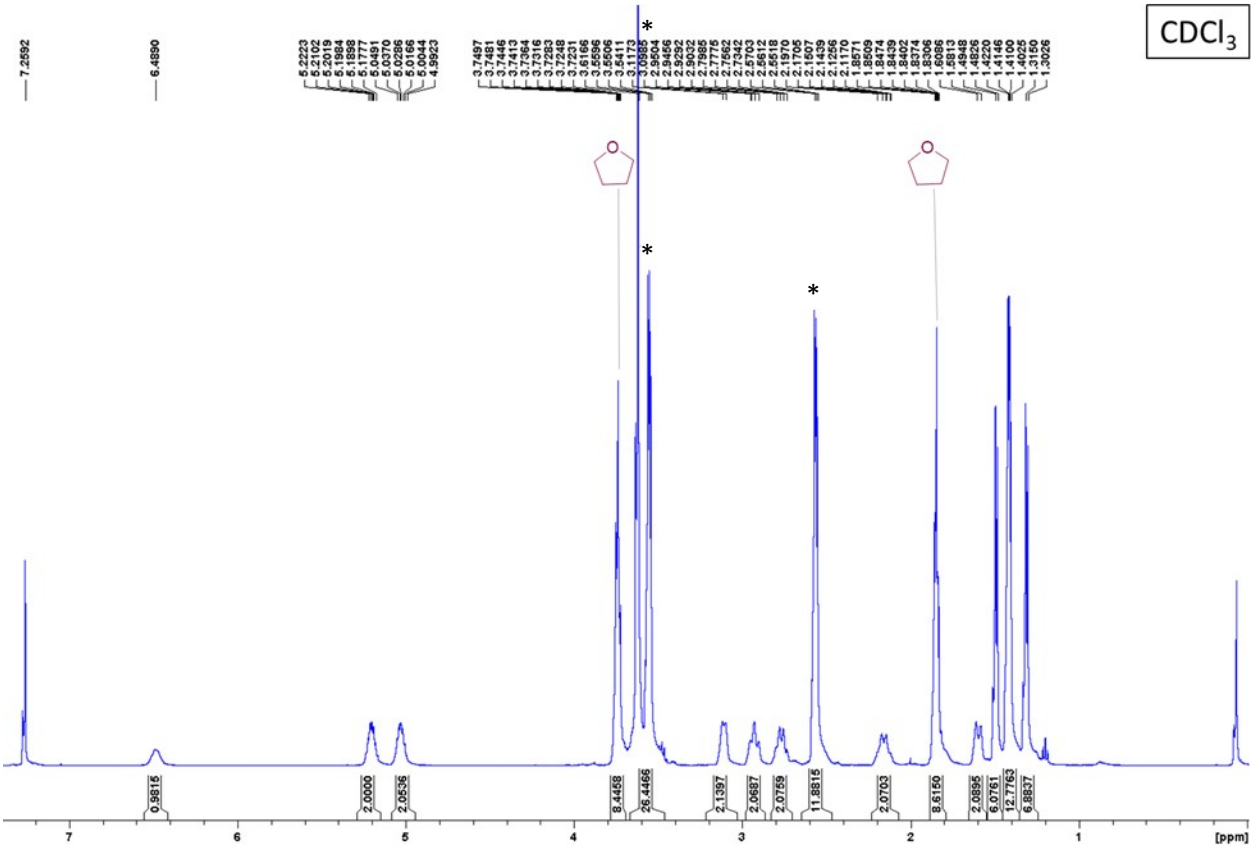

Figure S18. ^{1}H NMR spectrum of (^{iPrO}TBDPhos-HF)$PtCl_2$ (**3-HF**) in $CDCl_3$. The reaction byproduct Kryptofix 222®·KCl co-crystalizes with the sample, and resonances associated with Kryptofix 222® are assigned with an asterisk.

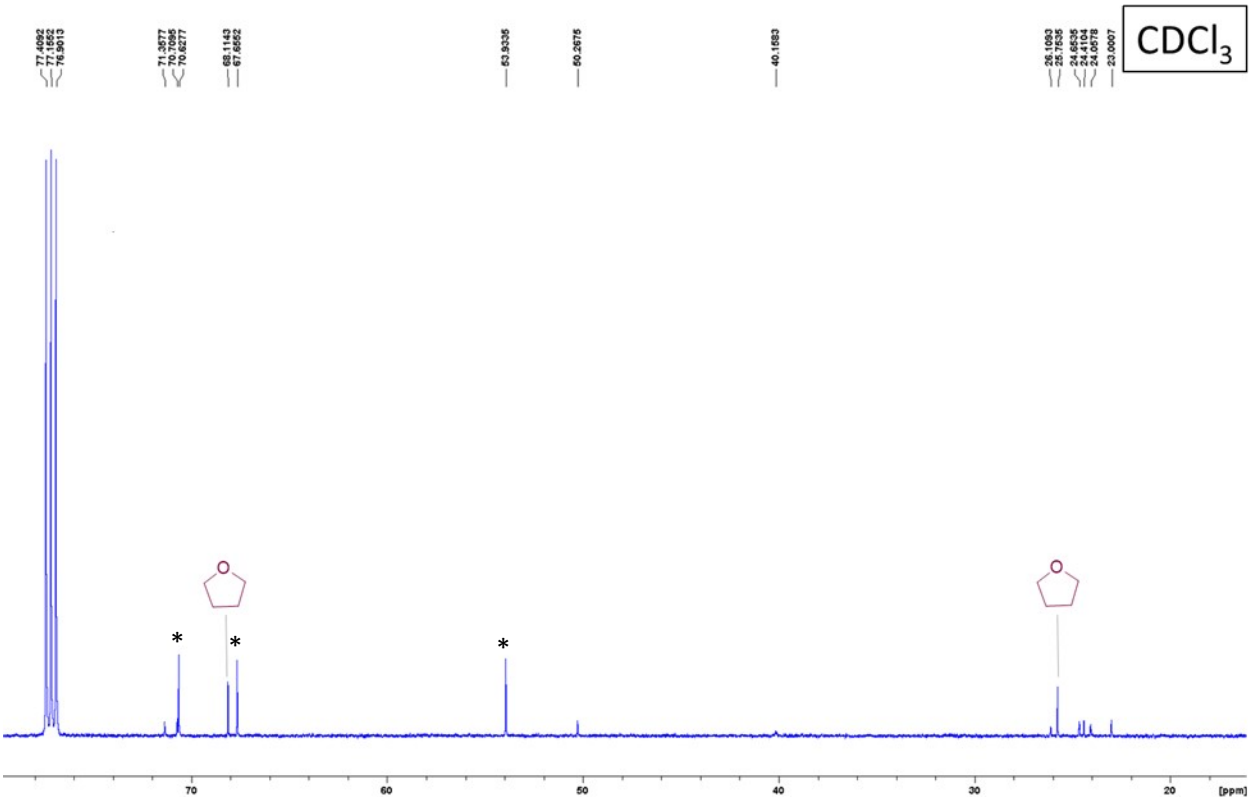

Figure S19. $^{13}C\{^{1}H\}$ NMR spectrum of (^{iPrO}TBDPhos-HF)$PtCl_2$ (**3-HF**) in $CDCl_3$. The reaction byproduct Kryptofix 222®·KCl co-crystalizes with the sample, and resonances associated with Kryptofix 222® are assigned with an asterisk.

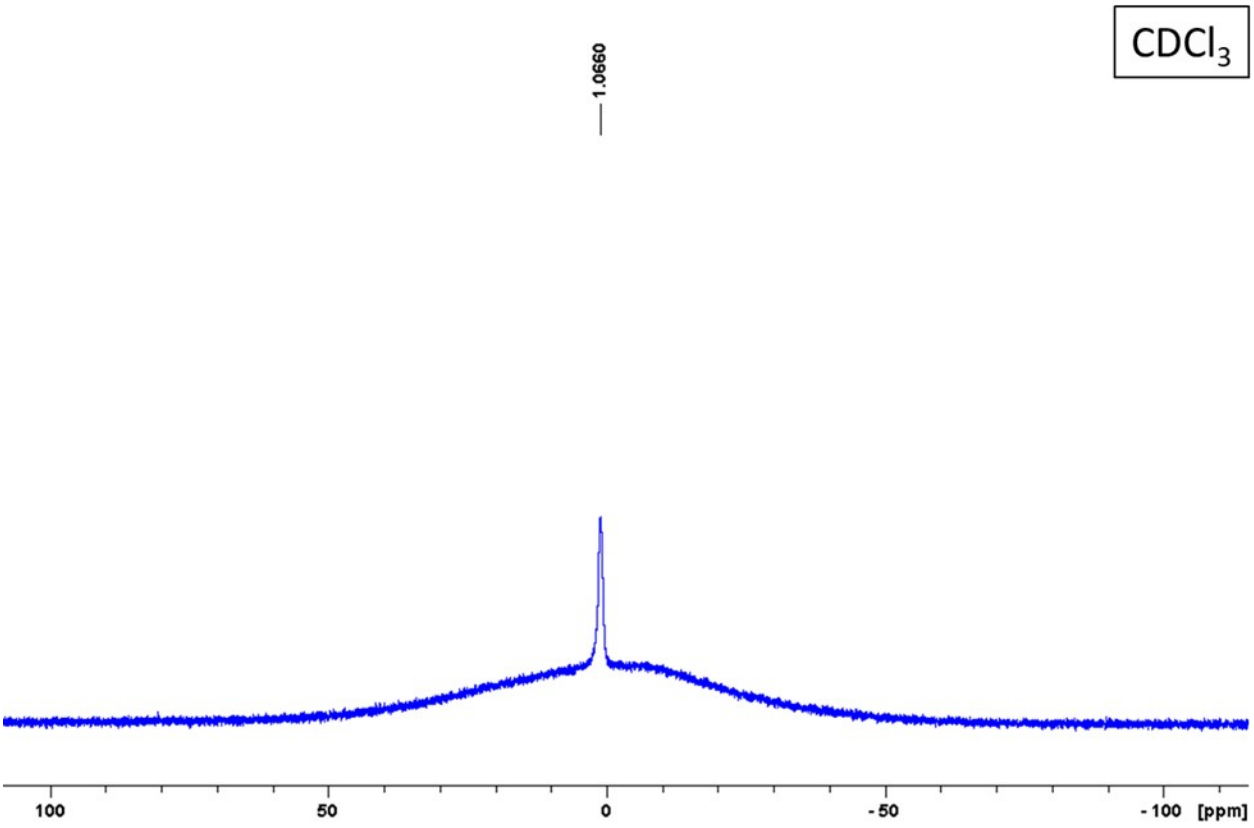

Figure S20. ^{11}B NMR spectrum of (^{iPrO}TBDPhos-HF)$PtCl_2$ (**3-HF**) in $CDCl_3$.

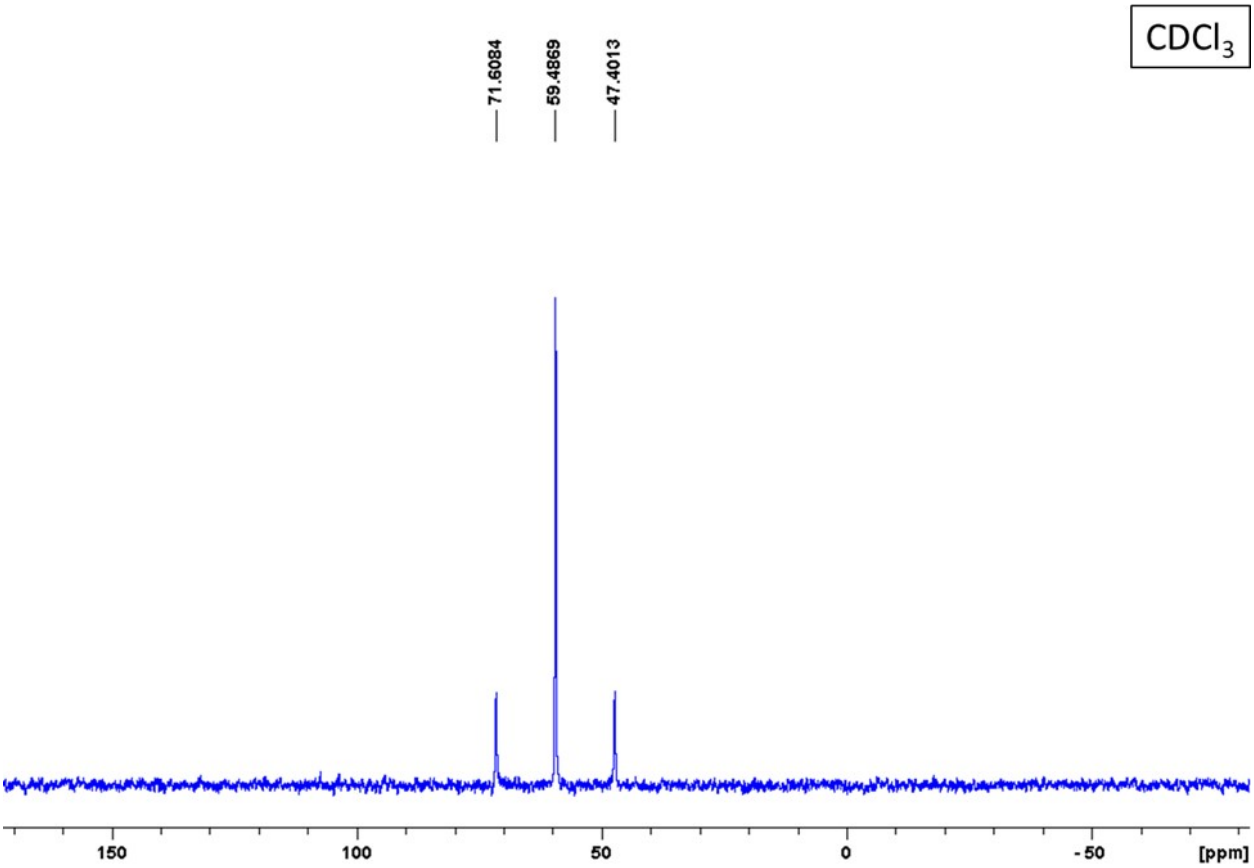

Figure S21. $^{31}P\{^{1}H\}$ NMR spectrum of (^{iPrO}TBDPhos-HF)$PtCl_2$ (**3-HF**) in $CDCl_3$.

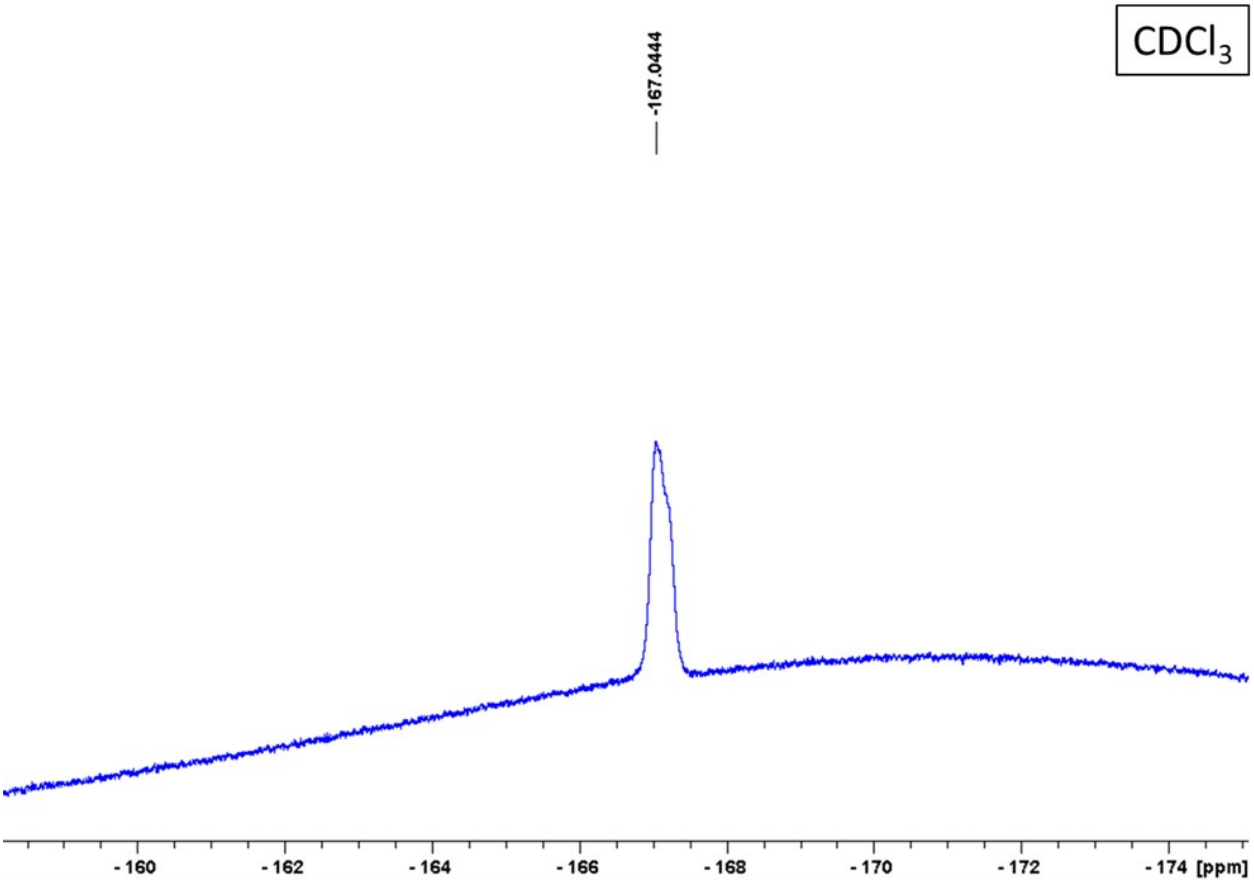

Figure S22. $^{19}F\{^{1}H\}$ NMR spectrum of (^{iPrO}TBDPhos-HF)$PtCl_2$ (**3-HF**) in $CDCl_3$.

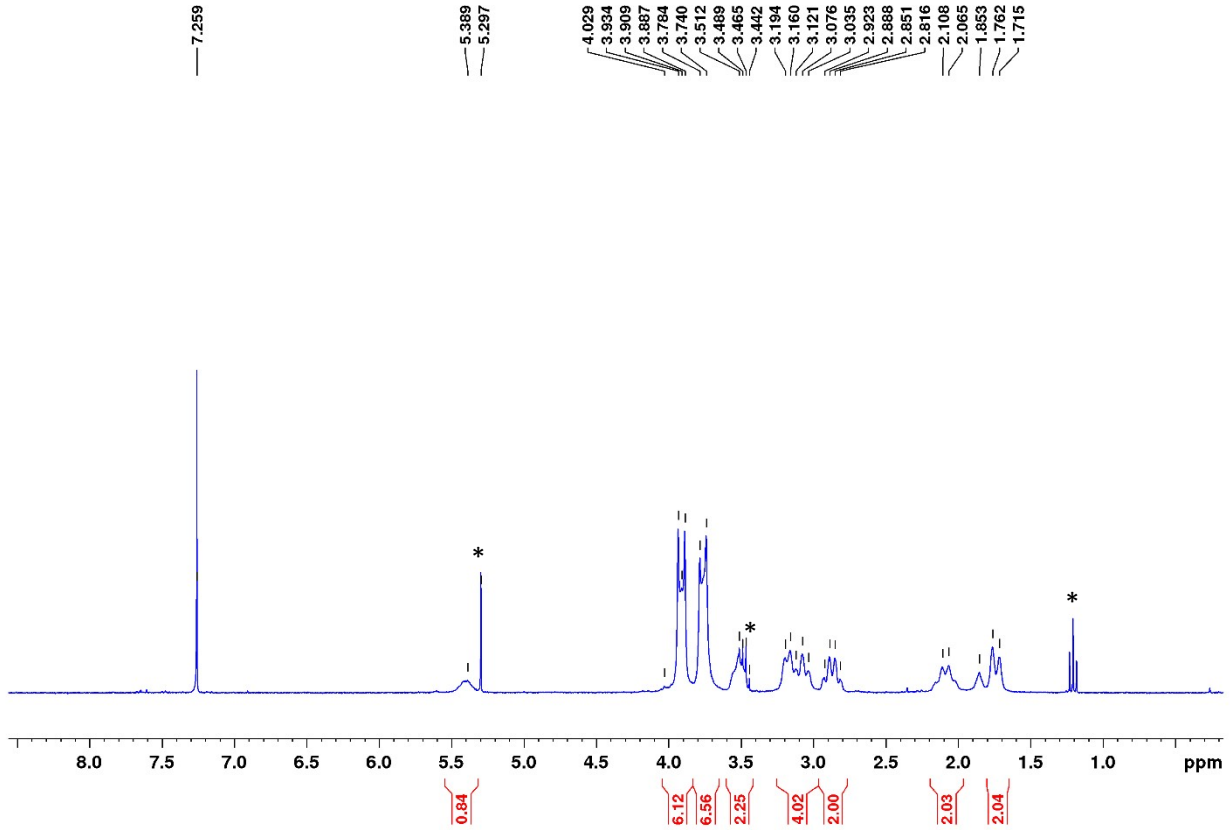

Figure S23. ^{1}H NMR spectrum of [(^{MeO}TBDPhos-HF)Pt(μ-Cl)]$_2$(BF_4)$_2$ (**4-HF**) in $CDCl_3$. The asterisk indicates resonances assigned to residual Et_2O and CH_2Cl_2.

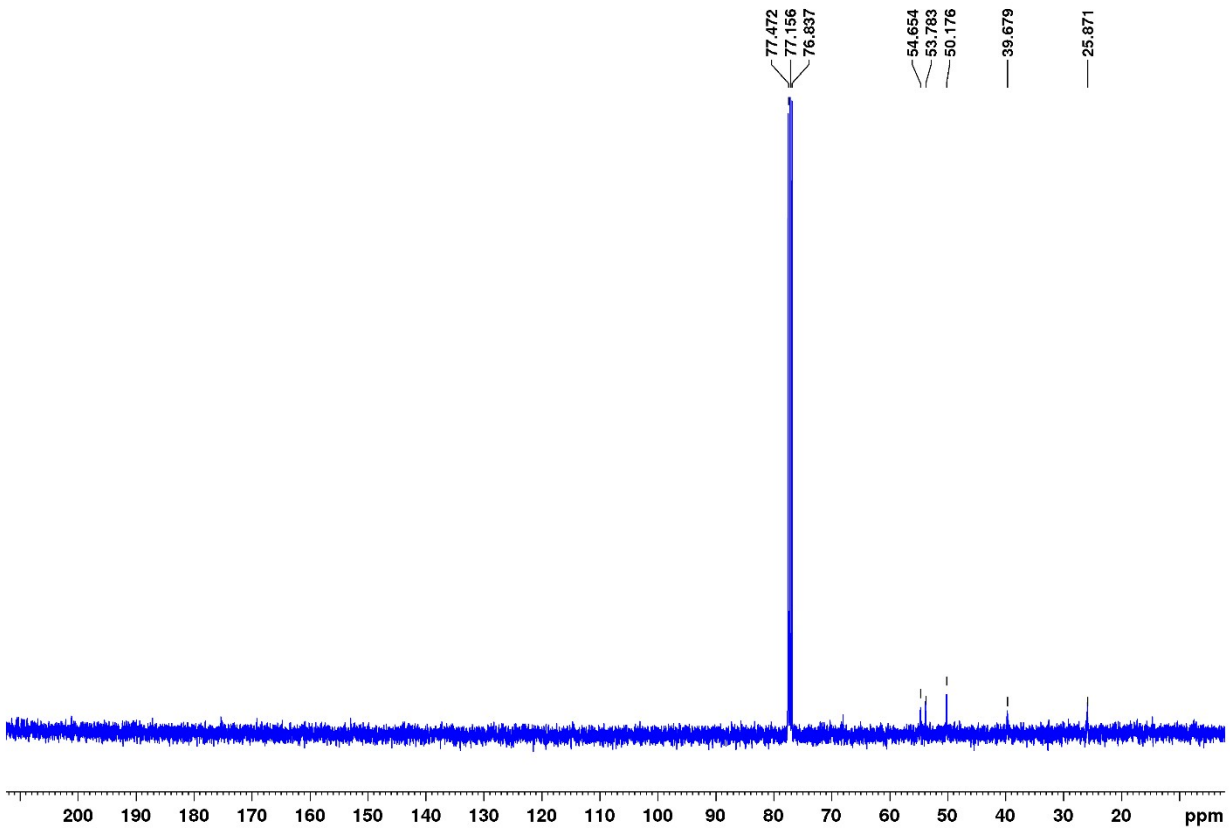

Figure S24. ^{13}C NMR spectrum of [(^{MeO}TBDPhos-HF)Pt(μ-Cl)]$_2$(BF_4)$_2$ (**4-HF**) in $CDCl_3$.

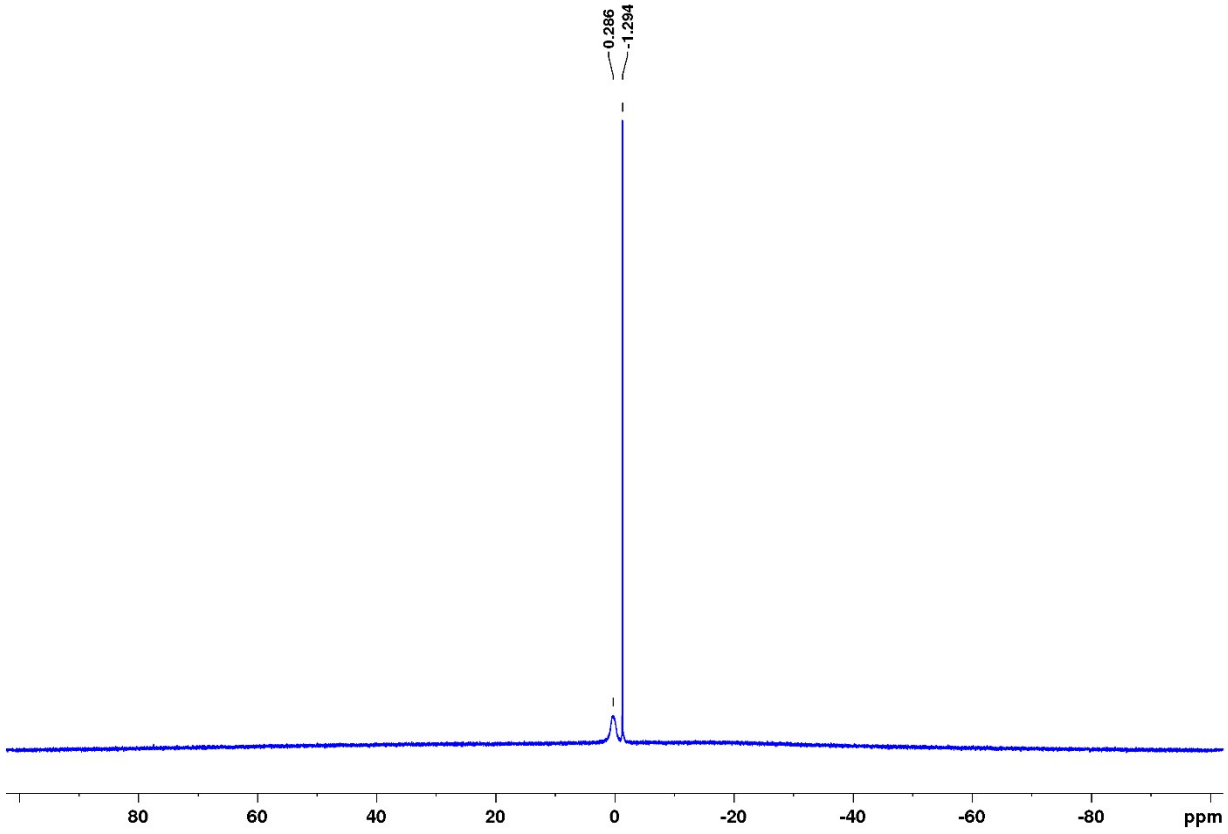

Figure S25. ^{11}B NMR spectrum of [(^{MeO}TBDPhos-HF)Pt(μ-Cl)]$_2$(BF_4)$_2$ (**4-HF**) in $CDCl_3$.

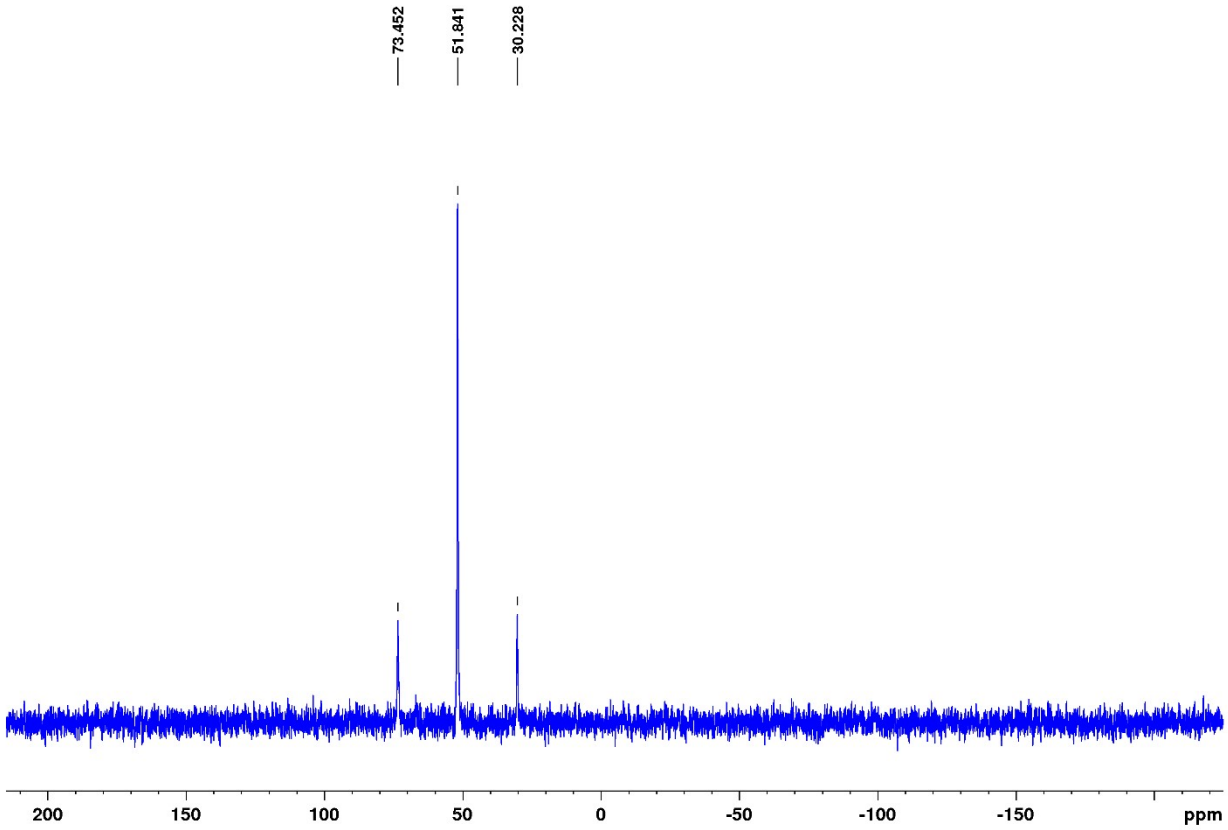

Figure S26. ^{31}P NMR spectrum of [(^{MeO}TBDPhos-HF)Pt(μ-Cl)]$_2$(BF_4)$_2$ (**4-HF**) in $CDCl_3$.

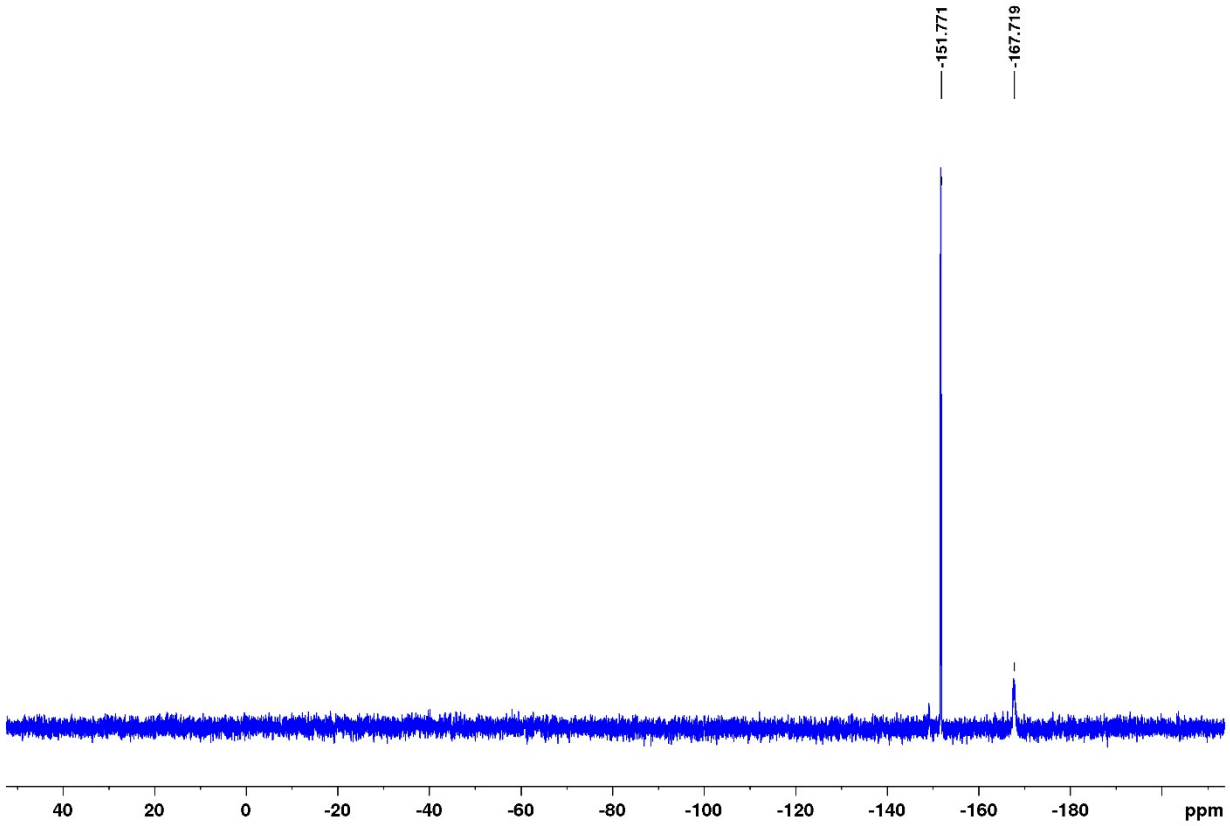

Figure S27. ^{19}F NMR spectrum of $[(^{MeO}TBDPhos\text{-}HF)Pt(\mu\text{-}Cl)]_2(BF_4)_2$ (**4-HF**) in $CDCl_3$.

3.2. NMR monitoring of **1** hydrolysis

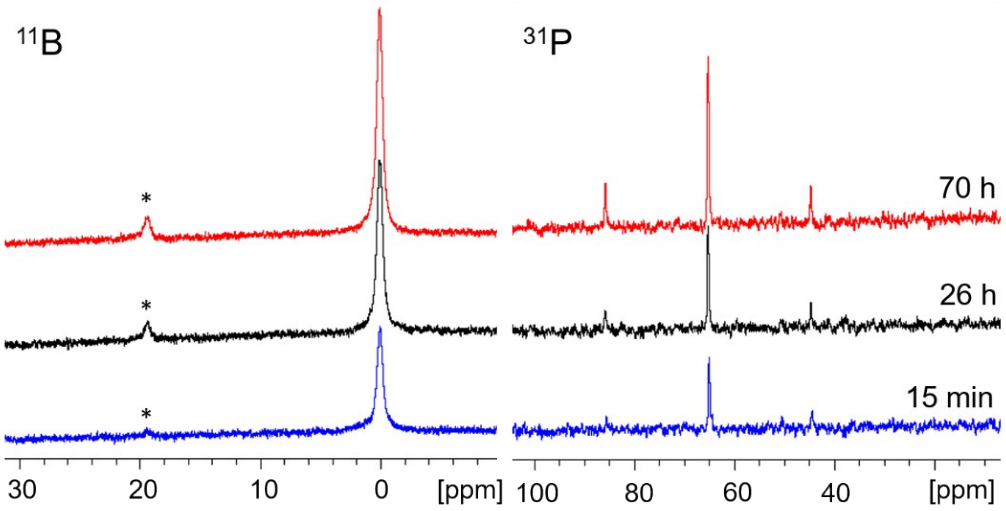

Figure S28. Time-resolved ^{11}B (left) and ^{31}P (right) NMR spectra of **1** in D_2O collected at 15 min (blue), 26 h (black), and 70 h (red). The asterisk symbols indicate resonances assigned to boric acid.

3.3. NMR monitoring of fluorination Method 1 (B-OH for B-F exchange)

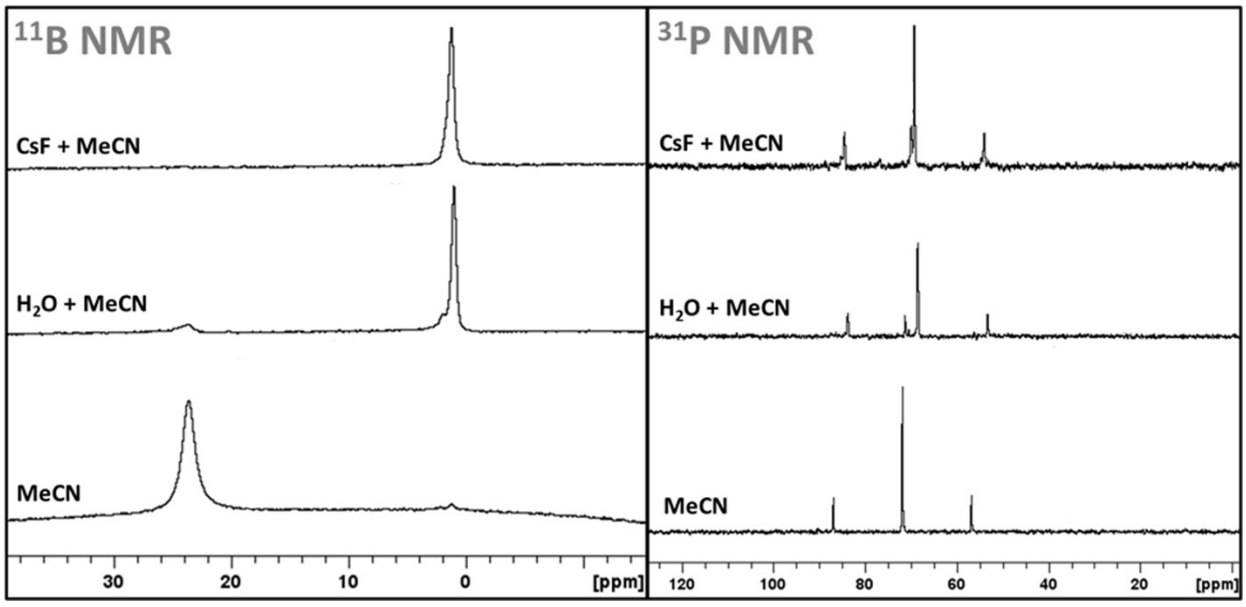

Figure S29. Overlay plot showing the ^{11}B and ^{31}P NMR spectra of **1** in MeCN (bottom), after addition of H_2O to form **1-H_2O** (middle), and after addition of CsF to the MeCN/H_2O solution containing **1-H_2O** (top).

3.4. NMR monitoring of **2-HF** hydrolysis

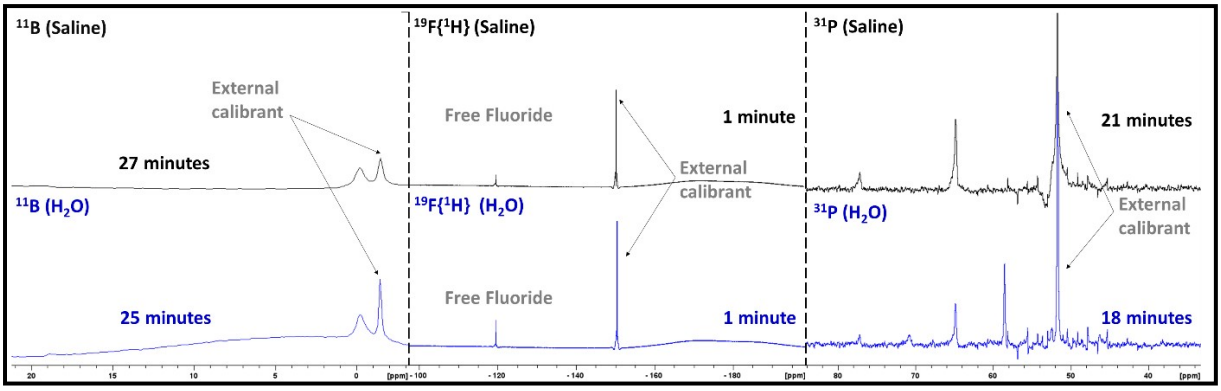

Figure S30. ^{19}F, ^{31}P, and ^{11}B NMR spectra of **1-HF** dissolved in water (blue) versus 0.90% w/v normal saline solution (black). The calibrant is (^{t}Bu$_3$PH)BF$_4$ in a sealed capillary.

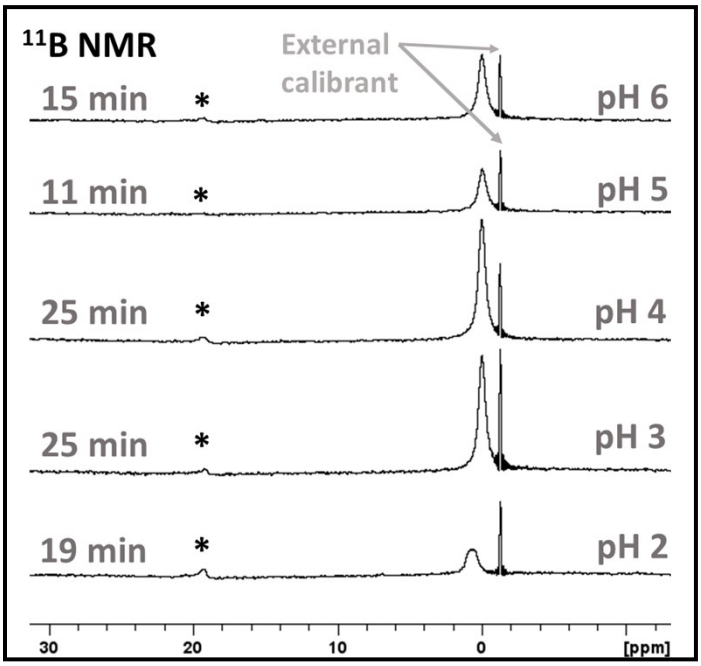

Figure S31. ^{11}B NMR spectra of **1-HF** collected in water at different pH (adjusted with HCl). The asterisks indicate peaks associated boric acid. The calibrant is (^{t}Bu$_3$PH)BF$_4$ in a sealed capillary.

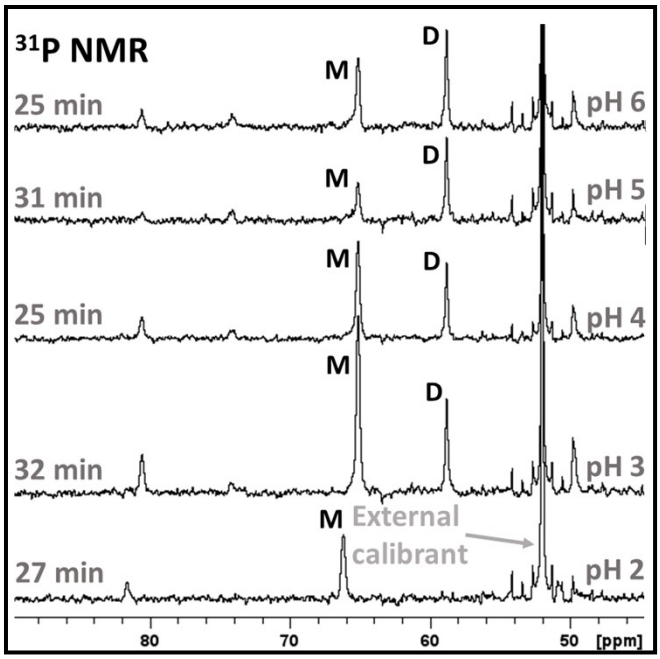

Figure S32. ^{31}P NMR spectra of **1-HF** collected in water at different pH (adjusted with HCl). The peak assigned as **M** indicates mononuclear whereas **D** corresponds to dinuclear. The calibrant is (^{t}Bu$_3$PH)BF$_4$ in a sealed capillary.

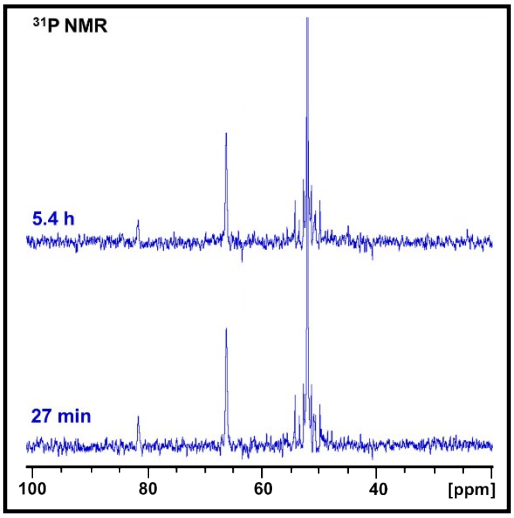

Figure S33. Time-resolved ^{31}P NMR screening of **1-HF** in water at pH 2.0. The calibrant is (^{t}Bu$_3$PH)BF$_4$ in a sealed capillary.

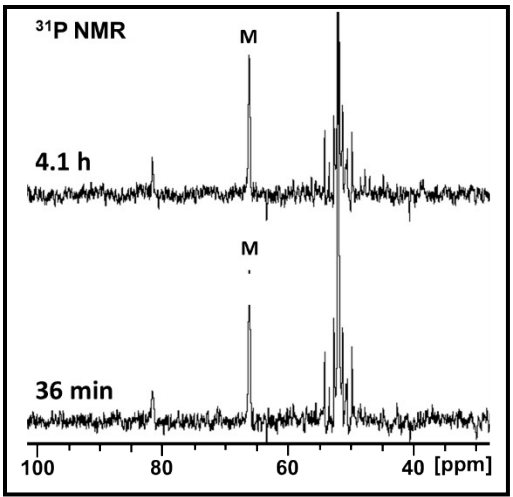

Figure S34. Time-resolved ^{31}P NMR screening of **1-HF** in saline at pH 1.5. The calibrant is ($^{t}Bu_3PH)BF_4$ in a sealed capillary.

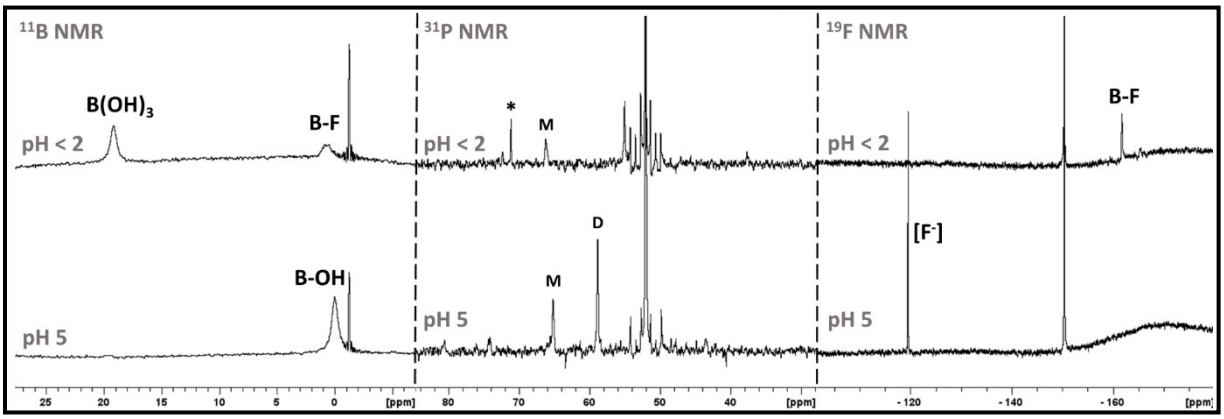

Figure S35. ^{11}B, ^{31}P, and ^{19}F NMR spectra of **1-HF** dissolved in 0.9% saline solution adjusted to pH 5.0 using HCl (bottom) and then after subsequent addition of HCl to lower the pH below 2 (top). The M and D labels correspond to mononuclear and dinuclear, respectively.

4. FT-IR spectra

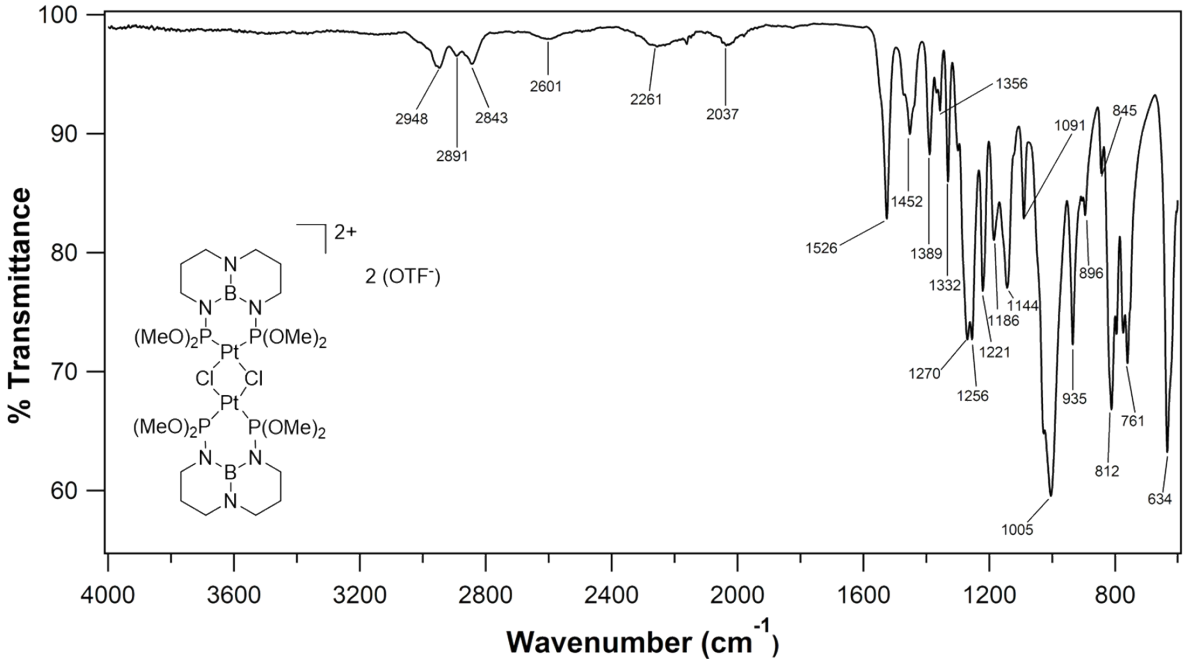

Figure S36. IR spectrum (ATR) of **2** collected in air.

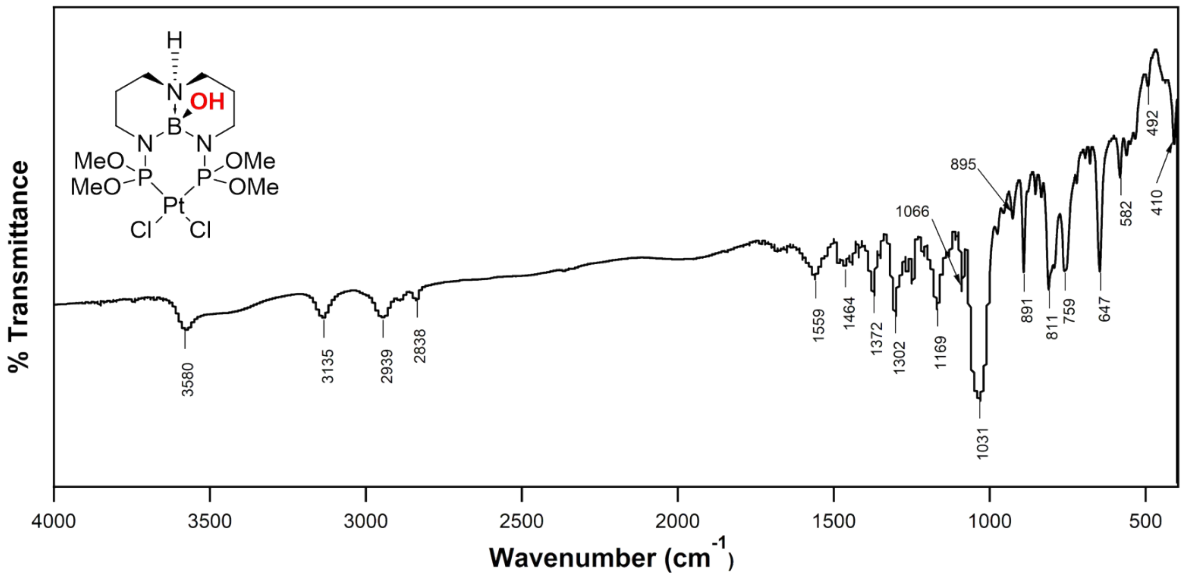

Figure S37. IR spectrum (ATR) of **1-H_2O** collected in air.

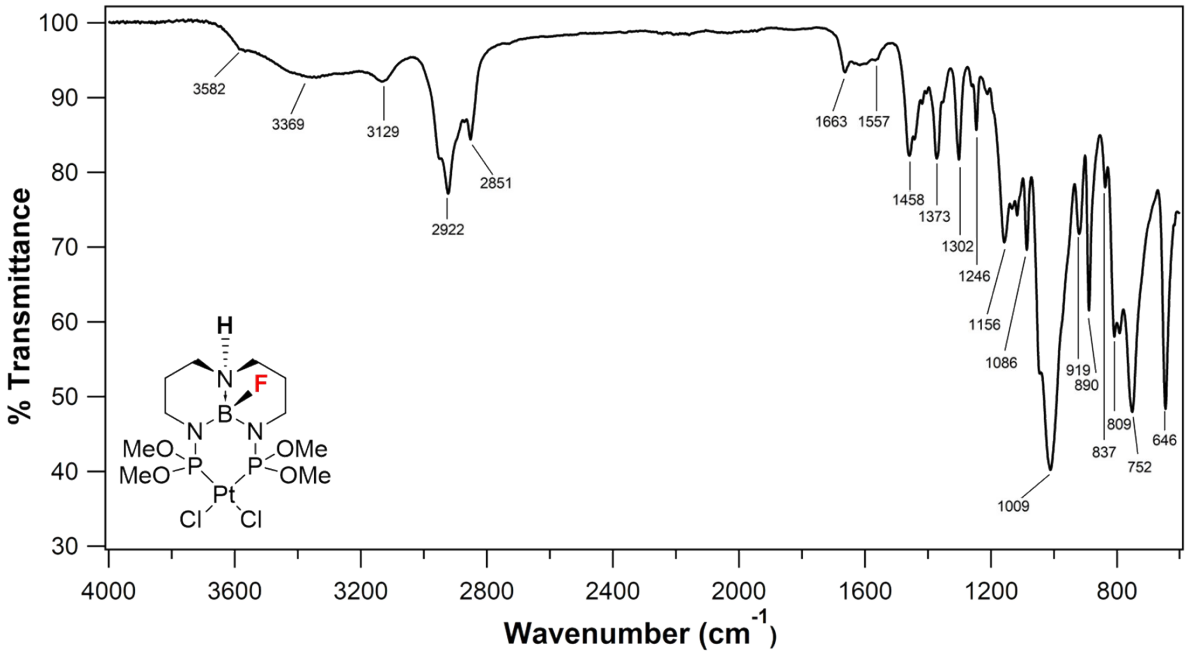

Figure S38. IR spectrum (ATR) of **1-HF** collected in air.

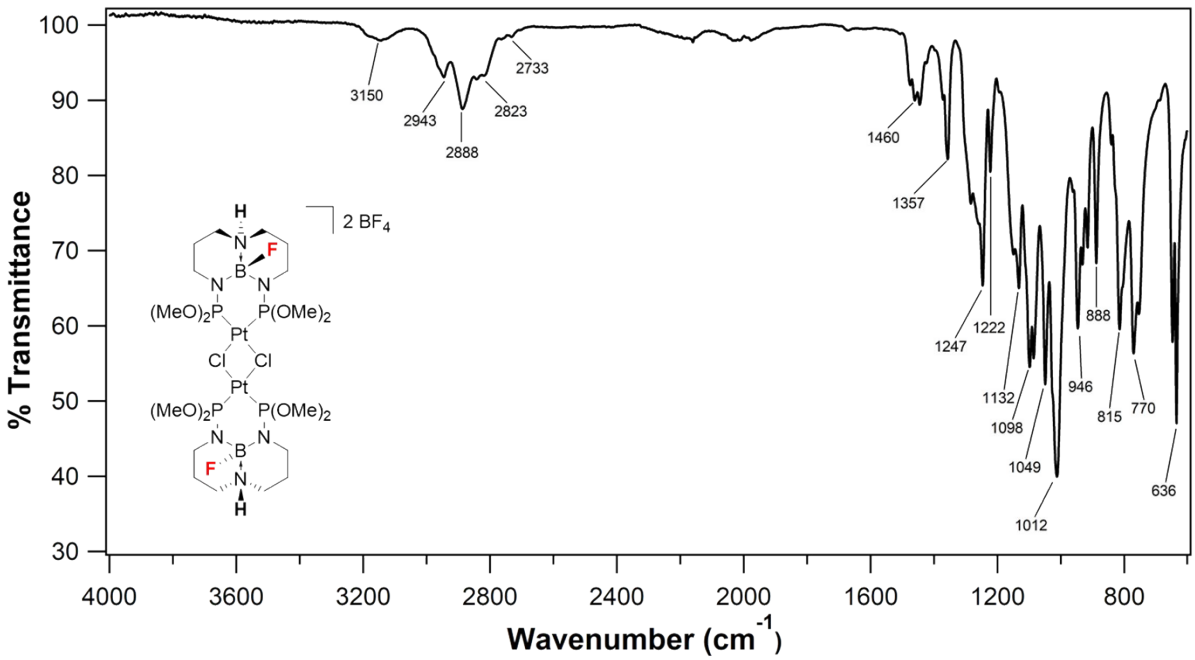

Figure S39. IR spectrum (ATR) of **4-HF** collected in air.

5. Supporting information references

(1) Lee, K.; Culpepper, J. D.; Parveen, R.; Swenson, D. C.; Vlaisavljevich, B.; Daly, S. R. *Organometallics* **2020**, *39*, 2526-2533.

(2) Culpepper, J. D.; Lee, K.; Daly, S. R. *Polyhedron* **2022**, *221*, 115877.

(3) Lee, K.; Wei, H.; Blake, A. V.; Donahue, C. M.; Keith, J. M.; Daly, S. R. *Dalton Trans.* **2016**, *45*, 9774-9785.

(4) Sheldrick, G. M. *Acta Crystallogr., Sect. A Found. Adv.* **2015**, *71*, 3-8.

(5) Sheldrick, G. M. *Acta Crystallogr., Sect. C Struct. Chem.* **2015**, *71*, 3-8.

(6) Dolomanov, O. V.; Bourhis, L. J.; Gildea, R. J.; Howard, J. A. K.; Puschmann, H. *J. Appl. Crystallogr.* **2009**, *42*, 339-341.

(7) Macrae, C. F.; Bruno, I. J.; Chisholm, J. A.; Edgington, P. R.; McCabe, P.; Pidcock, E.; Rodriguez-Monge, L.; Taylor, R.; van de Streek, J.; Wood, P. A. *J. Appl. Crystallogr.* **2008**, *41*, 466-470.